catalysts

MDPI

Review

Catalytic Reaction of Carbon Dioxide with Methane on Supported Noble Metal Catalysts

András Erdőhelyi

Institute of Physical Chemistry and Materials Science, University of Szeged, Rerrich Béla tér 1, H-6720 Szeged, Hungary; erdohely@chem.u-szeged.hu; Tel.: +36-62-343-638; Fax: +36-62-546-482

Abstract: The conversion of CO_2 and CH_4, the main components of the greenhouse gases, into synthesis gas are in the focus of academic and industrial research. In this review, the activity and stability of different supported noble metal catalysts were compared in the CO_2 + CH_4 reaction on. It was found that the efficiency of the catalysts depends not only on the metal and on the support but on the particle size, the metal support interface, the carbon deposition and the reactivity of carbon also influences the activity and stability of the catalysts. The possibility of the activation and dissociation of CO_2 and CH_4 on clean and on supported noble metals were discussed separately. CO_2 could dissociate on metal surfaces, this reaction could proceed via the formation of carbonate on the support, or on the metal–support interface but in the reaction the hydrogen assisted dissociation of CO_2 was also suggested. The decrease in the activity of the catalysts was generally attributed to carbon deposition, which can be formed from CH_4 while others suggest that the source of the surface carbon is CO_2. Carbon can occur in different forms on the surface, which can be transformed into each other depending on the temperature and the time elapsed since their formation. Basically, two reaction mechanisms was proposed, according to the mono-functional mechanism the activation of both CO_2 and CH_4 occurs on the metal sites, but in the bi-functional mechanism the CO_2 is activated on the support or on the metal–support interface and the CH_4 on the metal.

Keywords: supported noble metal catalysts; dry reforming of methane; CO_2 + CH_4 reaction; dissociation of CO_2

Citation: Erdőhelyi, A. Catalytic Reaction of Carbon Dioxide with Methane on Supported Noble Metal Catalysts. *Catalysts* **2021**, *11*, 159. https://doi.org/10.3390/catal11020159

Academic Editor: Zhixin Yu
Received: 19 December 2020
Accepted: 20 January 2021
Published: 23 January 2021

1. Introduction

Nowadays it is no longer necessary to emphasize that the increase of the CO_2—one of the main greenhouse gases—concentrations in the atmosphere and what kind of dangerous changes it can cause. To date, fossil fuels as the main sources of energy, the relatively new technologies (cement production, iron, steel industry etc.), the revolution in transportation, and the rapid growth in global population have resulted in the dramatic increase of CO_2 emission. Despite different international agreements CO_2 emissions have continued to increase. The CO_2 concentration in the atmosphere in the last few 100,000 years always remained below 300 ppm, but now the CO_2 concentration is over 415 ppm (in May 2020 the monthly mean value was 417 ppm) [1]. According to lots of meteorologists and climate experts, higher CO_2 concentration in the atmosphere results in climate change, the rise in temperature. The global annual mean temperature increased in the last 100 years by 1.4 degrees [2]. The climate change seems to have become generally accepted—although there are always those who disagree with it—and this has resulted in a worldwide increase in interest in reducing greenhouse gases, particularly CO_2, emissions.

If we want to prevent the increase of CO_2 concentration in the atmosphere we have to (i) hinder the enhancement of the carbon dioxide emission; (ii) use CO_2 capture and storage (CCS) technologies; or (iii) use CO_2 capture and utilization (CCU) technologies.

There is an ongoing debate as to whether CO_2 is a waste, or a wealth as feedstock. If CCS technology is used, CO_2 is considered waste, but if CO_2 is converted into a more valuable compound in a chemical reaction, it is not a waste but a feedstock.

The total amount of products that can be produced using technologies available today for CO_2 conversion is only a few hundred Mt, while CO_2 emissions from large stationary sources alone exceed 10 Gt. This means that traditional products and technologies do not really affect the CO_2 concentration in the atmosphere. One of the highest carbon emission sectors is transportation, so we have to look for the solution in these fields.

The reaction of carbon dioxide with methane, and dry reforming in particular utilizes two abundantly available greenhouse gases, to produce the industrially important syngas ($CO + H_2$ mixture). From the $CO + H_2$ mixture both fuel and methanol or plenty of other products can be produced using available technologies. This process could constitute a viable first step towards efficient CO_2 capture and utilization. The main problem is that dry reforming is a highly endothermic and equilibrium reaction (see later). However, CO hydrogenation is an exothermic process so these technologies could help in the storage of electricity because the greatest problem with renewable energy (wind and solar) production is the fluctuation, and the energy consumption is also uneven.

Opponents of the $CO_2 + CH_4$ reaction argue that carrying out this reaction requires a significant amount of energy. It is true that endothermic reaction consume energy. Synthesis gas is now produced worldwide by the steam reforming of CH_4, which is also an endothermic process and the dry reforming requires only 20% more energy, but converts greenhouse gases into a chemical feedstock. The disadvantage of steam reforming is that the H_2/CO ratio is too high to be used for methanol synthesis, although in the case of the $CO_2 + CH_4$ reaction this value is too low. The correct H_2/CO ratio could be obtained by reforming of methane with $CO_2 + H_2O$ mixture.

Extensive research work has been conducted on different catalytic systems for the conversion of $CO_2 + CH_4$, various catalysts have been developed but there have been only a few attempts to industrialize this reaction, so it is not surprising that the reaction of carbon dioxide with methane is in the focus of academic and industrial research.

The present review attempts to summarize the results obtained on supported noble metal catalysts. The main aim is to show the different results obtained on the similar catalysts, the different theories regarding the interaction of the reactants and the catalysts and the reaction mechanism.

2. The Thermodynamics of the $CO_2 + CH_4$ Reaction

Carbon dioxide reforming of methane is a highly endothermic reaction (1). Thermodynamic calculation indicates that this process is not spontaneous at 1 atm pressure below 906 K. When the reaction takes place between the products and between the products and the reactants, a number of secondary reactions can occur (2)–(7).

$CO_2 + CH_4 \rightleftharpoons 2\,CO + 2\,H_2$	$\Delta H^0_{298} = +247$ kJ/mol	dry reforming	(1)
$CH_4 + H_2O \rightleftharpoons CO + 3\,H_2$	$\Delta H^0_{298} = +206$ kJ/mol	steam reforming	(2)
$CH_4 \rightleftharpoons C + 2\,H_2$	$\Delta H^0_{298} = +75$ kJ/mol	methane decomposition	(3)
$CO_2 + H_2 \rightleftharpoons CO + H_2O$	$\Delta H^0_{298} = +41.2$ kJ/mol	reverse water–gas shift	(4)
$CO_2 + 4\,H_2 \rightleftharpoons CH_4 + 2\,H_2O$	$\Delta H^0_{298} = -164.9$ kJ/mol	methanation	(5)
$2\,CO \rightleftharpoons C + CO_2$	$\Delta H^0_{298} = -171$ kJ/mol	Boudouard reaction	(6)
$C + H_2O \rightleftharpoons CO + H_2$	$\Delta H^0_{298} = +131$ kJ/mol	carbon gasification	(7)

The calculated equilibrium conversions of methane and carbon dioxide at different temperatures are collected in Table 1 [3]. Similar results were obtained by Bradford and Vannice [4] for a feed stream at 1 atm total pressure ($CH_4/CO_2/He = 1/1/1.8$). The CO_2 conversion was always higher than that of methane, due to the reverse water gas shift reaction. The methanation (5) and the reverse reaction of steam reforming (2) may also have contributed to the lower methane conversion.

Table 1. The calculated equilibrium conversions at different temperatures for the CO_2 + CH_4 reaction at 1 atmosphere pressure [3].

Temperature K	CH_4 Conversion %	CO_2 Conversion %
673	6.9	9.9
773	25.6	32.9
873	57.7	66.8
973	84.0	89.6
1073	95.0	97.3
1173	98.3	99.2
1273	99.3	99.7

Different equilibrium conversions were calculated by Istadi and Amin [5] and by Nikoo and Amin [6]. The equilibrium methane conversion at 873 K was about 42% [5] while in the other work a value of 82% was reported [6]. The high CH_4 conversion in the latter case was explained by stating that the CH_4 decomposition (3) is the predominant reaction.

Figure 1 shows the equilibrium product distribution for the CO_2 + CH_4 reaction using CO_2/CH_4 feed ratio of 1/1 at a pressure of 1 atm [7]. This calculation cannot take into consideration the possibility of carbon deposition. According to this calculation water is formed up to 1173 K in the reaction and the CO/H_2 ratio is greater than one. These results indicate that the reverse water gas shift reaction also takes place.

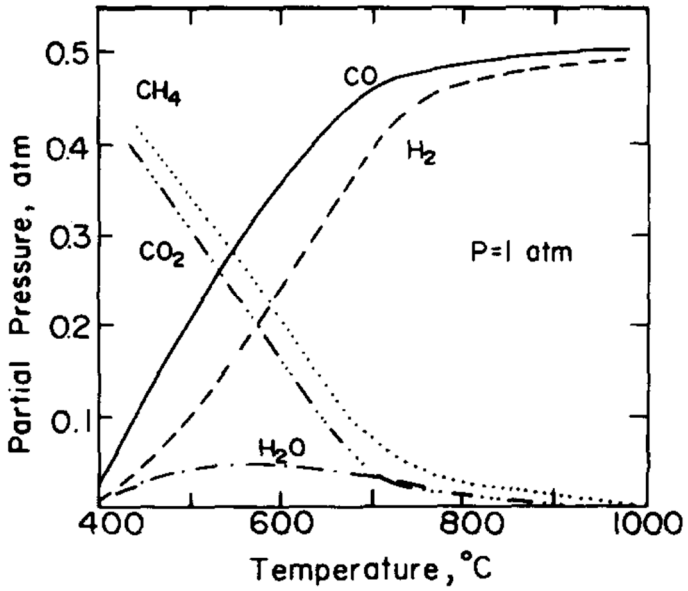

Figure 1. Composition—temperature diagram for the CO_2 + CH_4 reaction. (Reprinted with permission from [7] Copyright Elsevier 1986).

The reactions responsible for carbon formation are the methane decomposition (3) and the Boudouard reaction (6). Carbon formation cannot be ruled out in the hydrogenation of CO and CO_2. It was found [6] that of these processes only the methane decomposition is favored at high temperatures; while the other reactions are favored when the reaction takes place at lower than 800 K temperature.

When the carbon formation, i.e., the methane decomposition (3) and the Boudouard reactions (6), were taken into account in the calculation entirely different equilibrium composition was found (Figure 2) [8]. In this case the amount of H_2 is more than that of CO, the H_2/CO ratio is far greater than unity because the increased carbon formation lowers the amount of CO formed and hence increases the H_2/CO ratio.

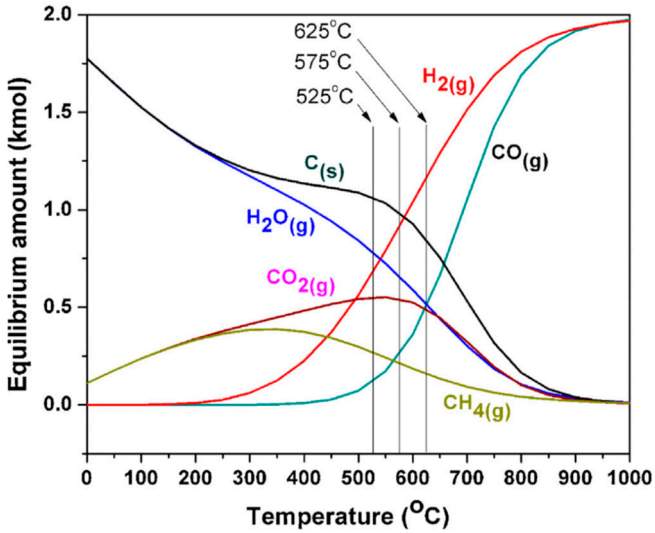

Figure 2. Thermodynamic equilibrium composition for 1 kmol of CH_4 and CO_2 each at 1 atm. (Reprinted with permission from [8]. Copyright Elsevier 2013).

According to Wang et al. [9] the reverse water–gas shift (4) and the Boudouard reaction (6) will not occur at above 1093 K, and the Boudouard reaction and methane decomposition (3) will be mostly responsible for the formation of carbon at temperatures ranging from 830 K to 973 K.

3. Comparing the Activity of Different Catalysts in the CO_2 + CH_4 Reaction

The possibility of a reaction between methane and carbon dioxide was already mentioned by Lang [10] in the late 19th century, and in 1928, Fischer and Tropsch [11] showed that different metals have different activities for the dry reforming of methane and that the group VIII metals show appreciable activity for this reaction. However, intensive research did not begin until the second half of the 20th century. Since then, a variety of different supported metals were used as catalysts. Most of the group VIII metals, except Os, are more or less active in the CH_4 + CO_2 reaction. The results obtained are summarized in different reviews [4,12–15]. The biggest problem was in most cases the rapid deactivation of the catalysts due to the significant carbon deposit. This may also be the reason of different activity orders published by different research groups. Catalysts based on noble metals are less sensitive to coking than Ni containing samples.

Theoretically the H_2/CO ratio is unit, but due to the reverse water gas shift reaction and to the other secondary reactions this ratio is often less.

The reforming reaction of CH_4 with CO_2 has been studied over different supported transition metals. It was found that at 1073 K the turnover frequencies (TOF) on Al_2O_3 supported catalysts (Ru, Rh, Pt, Ir, Ni) were within the same order of magnitude. The value obtained for the best Ru (4.0 s^{-1}) was only slightly more than twice as for the weakest Ni catalyst (1.8 s^{-1}) [16]. This order deviate from those found by Rostrup-Nielsen and Bak Hansen [17] who obtained Ru > Rh $\geq$ Ni > Ir > Pt > Pd order (Table 2).

Table 2. Comparison of turnover frequencies of supported noble metal catalysts for CO_2 reforming of methane.

	Al_2O_3 CO_2/CH_4 = 1/1.5 1073 K [16]	Al_2O_3 CO_2/CH_4 = 1/1 973 K [17]	Al_2O_3 CO_2/CH_4 = 1/1 823 K [18]	Alumina Stabilized Magnesia CO_2/CH_4 = 4/1 823 K [19]	Al_2O_3 CO_2/CH_4/He = 1/1/8 723 K [20]
Ru	4.0	2.0	1.36	2.9	0.2
Rh	3.4	4.0	0.32	1.9	0.8
Pd		< 0.1	0.64	0.18	
Ir	2.0	2.0	0.18	0.44	0.5
Pt	3.8	< 0.1	0.36	0.36	0.2
Ni	1.8			1.9	0.6

No significant differences were found at 1050 K in the activities of the alumina supported metal catalysts [21,22] only in the cases of Ru and Pd were significantly lower conversions observed; in the other cases they approached the equilibrium values. The Ni and Pd catalysts were very active at first (especially Ni), then rapidly showed a decline in conversions, and a considerable deposition (up to 40%) of carbon occurred within a few hours. The Ir/Al_2O_3 catalyst maintained its very high performance for over 200 h, with no evidence for deactivation, and only less than 0.3% carbon was observed on the used catalyst.

The order of catalytic activity at 723 K on turnover frequency basis was found to be Rh > Ni > Ir> Ru~Pt > Co over the alumina supported catalysts [20] (Table 2). A different sequence was found for SiO_2 supported metals: Ni > Ru > Rh~Ir > Co~Pt [20]. This indicates that the support has a great influence on the specific activity of the catalysts.

Over different MgO supported metal catalysts the activities depended upon the metals in the sequence Ni, Ru, Pt >> Rh > Pd [23]. The amounts of CO were greater than those of H_2 possibly due to the reverse water gas shift reaction. Different results were obtained at 1073 K on MgO supported noble metals [24]. The methane conversion was the highest on Rh and the activity decreased following the order Rh > Ru > Ir > Pt > Pd.

CO_2 reforming of CH_4 has been also studied on catalysts containing less than a monolayer of Rh, Ru, and Ir deposited on α-Al_2O_3, MgO, CeO_2, La_2O_3, and TiO_2 [25]. It was found that the activity, the turnover frequency of CH_4 consumption on Rh/α-Al_2O_3 was four times higher than on Ru and Ir. The high stability of the noble metal catalyst comparing with the Ni was attributed to the high oxidative properties of compounds formed on the catalyst surface, which inhibit the carbon growth reactions [25].

The turnover frequency for CO formation in the dry reforming of CH_4 on SiO_2 and TiO_2 supported transition metals depends on both the support and the %-d character of the metal [26]; however, different trends were observed for metals on SiO_2 and TiO_2. The activities of the TiO_2 supported metals were higher than those of SiO_2 based catalysts in all cases. Pt/SiO_2 has an outstanding activity among the silica supported samples and it decreased in the following order at 723 K: Pt >> Pd > Ni > Rh > Fe. Among the TiO_2 supported catalysts the Rh activity was the highest. In this case the turnover frequency for CO formation decreased in the Rh > Ir > Ru > Pt > Pd > Ni > Fe~Co~Cu order [26].

The methane conversion at 923 K decreased on pillared clay impregnated by different metals along the 3% Rh > 10% Ni > 3% Pd > 3% Ni > 3% Ce sequence [27]. The H_2/CO ratio was 1.1 for Rh and 0.85 for Pd which is metallic at the temperature of the reaction but it was even lower for Ni and Ce.

Comparing the activities of the $ZnLaAlO_4$ supported Ru, Ni, and Pt catalysts reveals that the best performance was observed for 3% $Ru/ZnLaAlO_4$ while the 3% Pt shows the lowest activity. These results were attributed to the synergistic effect of the interaction between the support and the active metals [28].

Only the activities of noble metals have been compared in several publications [18,29–33] and great differences were found in their catalytic behavior as concerns the CH_4 + CO_2

reaction. The reaction occurred at the highest rate on Rh, followed by Pt, Pd, Ru, and Ir. Little or no deactivation of the catalyst occurred during the reaction at 823 K.

The conversion of CO_2 exceeded that of CH_4 for every catalyst sample indicating that the dry reforming reaction was followed by several secondary processes, including the methanation of CO_2 and CO, reverse water gas shift reaction and the Boudouard reaction. The turnover frequency for CH_4 or CO_2 consumption at 823 K on the alumina supported 1 wt% of noble metals decreased in the sequence Ru > Pd > Rh > Pt > Ir [18] (Table 2). This is practically the same as the order for CO methanation [34], and the sequence for CO_2 methanation differed only in that Pd was the least active sample [35]. In contrast at 923 K the order Rh > Ru > Ir >> Pd, Pt was determined for catalysts with 0.5% metal supported on Al_2O_3 [17] (Table 2) but others found that the activity decreased in the order Rh > Pd > Pt >> Ru [29]. Rh, Ru, and Ir catalysts showed stable long term activity but Pd and Pt containing catalysts deactivated rapidly. On alumina-stabilized magnesia and Mg-Al mixed oxide supported Pt metals at 973 K a different sequence was observed [30,32,33] (Ru > Rh > Ir > Pt > Pd).

The order of activities for ZrO_2-supported catalysts was Rh > Pt > Ir, Pd > Ru [36]. This sequence is different from that reported for MgO-supported materials [19,24]. The observed differences suggest that the basicity of the support may have some significant effect.

Stable CH_4 and CO_2 conversion was observed for 50 h on Ru substituted $LaAlO_3$ ($LaAl_{0.98}Ru_{0.02}O_{3-\delta}$) catalyst. This indicates that it is a highly stable and coke resistant catalyst. It has been suggested that the thermal stability of the sample is due to a strong interaction between Ru and Al. In contrast, Pt and Pd incorporated into $LaAlO_3$ lost their activities due to sintering and carbon deposition [37].

The activities of Rh, and Pt supported α-Al_2O_3 doped with La_2O_3 and BaO were compared in the dry reforming of methane [38]. It was found that Rh is more active than Pt independently of the support composition. La incorporation induces a rate enhancement in the conversion of methane in all cases, but Ba incorporation in Pt/Al_2O_3 leads to loss of activity because there is a preferential interaction between Pt and Ba, in the case of Rh this had no effect.

Ru- and Rh-catalysts supported on Mg-Al mixed oxides revealed activity in the combined partial oxidation and dry reforming of methane to synthesis gas at 1123 K which was markedly higher than that of Pt. Ru and Rh approached their maximal activity which was limited by the equilibrium [39].

Ru and Ir supported on Eu_2O_3 were active in the dry reforming reaction, but Ru showed an onset of activity around 673 K, whereas the Ir showed initial activity at a much higher temperature, around 823 K [40].

The activity of $BaZr_{(1-x)}Me_xO_3$ (Me: Ru, Rh, Pt) perovskite type oxides [41] decreased with the active species as Rh > Ru > Pt. The better activity of Rh- and Ru-containing samples was linked to their highl- reducible nature.

The brief summary above clearly shows that noble metals are effective in the CO_2 + CH_4 reaction. Despite the high costs of noble metals, their superior catalytic properties at low temperature still make them indispensable to understand the interaction between the metal and the support, to check the surface compounds formed during the reaction and to show the elementary steps of the reaction, and as additives appear to be unavoidable for the development of an effective and stable catalyst.

4. Dry Reforming of Methane on Supported Noble Metal Catalysts

4.1. Supported Rhodium

The above summary clearly shows that Rh is one of the best and most stable catalysts of the reaction.

The specific activity of Rh catalysts was found to strongly depend on the support [42–45]. It decreased in the order yttria-stabilized zirconia (YSZ) > Al_2O_3 > MgO > TiO_2 > SiO_2 [43,44]. This order correlates directly with the acidic character of the support [43]. A strong dependence was observed on the specific activity of the methane

reforming reaction and the rate of deactivation of the catalysts on rhodium particle size in the range 1–6 nm. Both activity and rate of deactivation decrease with increasing metal particle size. The degree of these dependencies was largely affected also by the nature of the support. Relatively high deactivation rates were observed over Rh/TiO_2 and on Rh/MgO, but on Rh/YSZ and on Rh/SiO_2 no deactivation was observed. Three kinds of factors were suggested which contribute to the catalyst deactivation carbon deposition, metal sintering, and the poisoning of surface Rh sites by species originating from the carrier [43]. The TOF for 0.5% Rh/YSZ at 923 K was about five times higher than for the less active SiO_2 or TiO_2 supported catalysts in the steady state [44].

Others found no significant difference in the catalytic activity at 773 K on 1% Rh supported on $A1_2O_3$, TiO_2, SiO_2, MgO (Table 3) and no decay in the activity was experienced and small amount if any carbon deposit was observed [46].

Table 3. Turnover frequencies on different supported Rh catalysts in the $CO_2 + CH_4$ reaction.

Catalyst	Temperature K	N_{CH_4} s^{-1}	N_{CO_2} s^{-1}	N_{CO} s^{-1}	N_{H_2} s^{-1}	References
Rh/Al_2O_3	723			0.52		[47]
Rh/TiO_2	723			0.29		[47]
Rh/Nb_2O_5	723			0.48		[47]
Rh/NaY	723			0.08		[47]
3.8% Rh/SiO_2	723	0.08		0.18		[48]
3.3%$Rh/VO_x/SiO_2$	723	1.3		3.4		[48]
1% Rh/Al_2O_3	773			0.39	0.15	[46]
1% Rh/MgO	773			0.85	0.5	[46]
1% Rh/TiO_2	773			0.37	0.22	[46]
1% Rh/SiO_2	773			0.32	0.2	[46]
1% Rh/α-Al_2O_3	873	1.5				[17]
1% Rh/ZrO_2	873	0.9				[17]
1% Rh/TiO_2	873	1.3				[17]
1% Rh/SiO_2	873	1.2				[17]
Rh/γ-Al_2O_3	875		4.6			[49]
Rh/SiO_2	875		1.2			[49]
0.5% Rh/Al_2O_3	893	25.5				[50]
0.5% Rh/SiO_2	893	6.1				[50]
0.5% Rh/Al_2O_3	1013	6.35				[45]
Rh/α-Al_2O_3	1023	5.02	5.08			[25]
Rh/MgO	1023	1.04	1.06			[25]
Rh/CeO_2	1023	2.82	3.04			[25]
Rh/TiO_2	1023	0.74	0.85			[25]
Rh/La_2O_3	1023	4.01	4.06			[25]

In contrast a significant effect of the support was found on the reaction rate on Rh supported on the same oxides, where the order was $Rh/Al_2O_3 > Rh/TiO_2 > Rh/SiO_2$. The catalytic activity of Rh/SiO_2 increased significantly by physically mixing the catalyst with metal oxides such as $A1_2O_3$, TiO_2, and MgO, indicating a synergistic effect. The role of the metal oxides used in mixture according to the authors may be ascribed to promoting in dissociation CO_2 dissociation on the surface of Rh, since the $CH_4 + CO_2$ reaction is first order in the pressure of CO_2, and -0.6 for CH_4, suggesting that CO_2 dissociation is the rate-determining step [50,51].

The reforming of methane with carbon dioxide was investigated on Rh supported on reducible (CeO_2, Nb_2O_5, Ta_2O_5, TiO_2, and ZrO_2) and on irreducible (γ-Al_2O_3, La_2O_3, MgO, SiO_2, and Y_2O_3) oxides [45]. The reducible oxides supported Rh provided much lower conversion of CH_4 or CO_2 than the irreducible one. One possible explanation is that the Rh particles were partially covered by partially reduced oxide species (SMSI effect). Among the irreducible oxides supported catalysts, γ-Al_2O_3, La_2O_3, and MgO showed stable activities, and it increased in the sequence: $La_2O_3 < MgO \approx \gamma$-$Al_2O_3$. Possible

explanations for stability, based on the strong interactions between Rh_2O_3 and support were proposed. Among the reducible oxides, Nb_2O_5 supported Rh has a low activity, Rh/ZrO_2 and Rh/CeO_2 exhibited a very long activation period, and deactivation occurred over Ta_2O_5 and TiO_2. MgO and γ-Al_2O_3 supported Rh are the most promising catalysts; they provided a stable high activity with a CO yield of 83–85% and a H_2 yield of 76–79% at the high space velocity of 60 000 mL/h/g [45].

The turnover frequency for methane conversion in the $CO_2 + CH_4$ reaction on different oxide supported Rh catalysts decreased in the following order: $Rh/TiO_2 > Rh/La_2O_3 = Rh/CeO_2 > Rh/ZrO_2 = Rh/MgO = Rh/SiO_2 = Rh/MCM\text{-}41 > Rh/Al_2O_3$. The outstanding activity of Rh/TiO_2 was attributed to the fact that Rh remained in metallic state during the reaction, while on Rh/Al_2O_3 according to XANES characterization cationic Rh was generated [42].

The highest yield in hydrogen in the dry reforming of CH_4 was obtained on differently doped alumina supported Rh in the following order: $Rh/NiO\text{-}Al_2O_3 > Rh/MgO\text{-}Al_2O_3 \sim Rh/CeO_2\text{-}Al_2O_3 > Rh/ZrO_2\text{-}Al_2O_3 > Rh/La_2O_3\text{-}Al_2O_3$. The high activity of $Rh/NiO\text{-}Al_2O_3$ was explained by the presence of $NiAl_2O_4$ spinel preventing the deactivation of Rh migration in alumina and the high dispersion of Rh favored by the presence of Ni particles at the support [52].

Rh/NaY effectively catalyzes the conversion in the $CO_2 + CH_4$ reaction to CO and H_2 with a H_2/CO ratio near unity even with low metal loadings [53,54]. Remarkable is the stability of these catalysts under operating conditions. The reason for this, according to the authors is the total absence of carbonaceous deposits. The Rh particles are quite uniform, having a size of~4 nm [53]. These particles are available in the early stages of the catalysis and the zeolite framework protects the encaged particles against further growth. Therefore, catalyst deactivation is not observed under these conditions which are significant for Rh on amorphous supports [53,54].

Unlike other results [54,55] no carbon formation was observed on Rh/Al_2O_3 in the temperature range of 873–1073 K [56]. Although the activity of the catalyst decreased slightly over time, this was attributed to the sintering because the catalysts could not be regenerated. This catalyst has been successfully tested in large scale experiments in solar panels. The reforming reaction at 923 K over Rh/Al_2O_3 results in the accumulation of three kinds of carbon species. The ratio of different carbon species depended on the reaction temperature and on the time of exposure. These results support the earlier finding that the transformation of the active form into a less active form occurs with increasing reaction time and the temperature [57]. The amount of carbon deposit decreased at temperatures higher than 923 K probably because of the prevalence of the carbon gasification (8) and the reverse Boudouard reaction (6). It was found that the origin of carbon is mainly the CO_2 molecule, with a small contribution from the CH_4 molecule [44,55].

Bitter et al. [49] also found that the activity of supported Rh catalysts for $CO_2 + CH_4$ reaction is mainly determined by the availability of Rh irrespective of the support. Contrary to this, Portugal et al. [57] found that the turnover frequency for CO formation over supported Rh at 723 K is strongly affected by the support; it decreased in the following order: $Rh/Al_2O_3 > Rh/Nb_2O_5 > Rh/TiO_2 > Rh/NaY$ (Table 3). The higher activity of the oxide-supported catalysts was explained by the higher degree of contribution of the reverse water–gas shift reaction. Similarly, a dominant role of the carrier was observed, the turnover frequency for CH_4 or CO_2 consumption at 1023 K decreased in the $Rh/\alpha\text{-}Al_2O_3 > Rh/La_2O_3 > RhCeO_2 > Rh/MgO > Rh/TiO_2$ order [25] (Table 3).

Alumina supported Rh catalysts with a wide range of dispersions (25.1–69.0%) and Rh particle size (1.4–4.0 nm) were prepared by varying the metal content (0.1–1.6 wt%) and the thermal treatment temperature (923–1123 K) [58]. It was found that the turnover rates increased monotonically with increasing Rh dispersion. A similar result was obtained on different NaY zeolite supported Rh, too [47]. This observation suggests that coordinative unsaturated Rh surface atoms, which are more common in small clusters, are more active than those in low-index surface planes on larger Rh crystallites. Edge and corner atoms

appear to bind CH_x and H more strongly and to decrease the energy required to form relevant transition states for the initial C–H bond activation. They assume that supports can influence metal dispersion and, only in this manner, affect forward turnover rates [58]. It should be noted that a reduction of Rh particle size result in an enhanced rate of deactivation in the case of supported Rh [43].

Contrary to the above findings, it was found that over a wide range of metal content of the catalysts (0.5–5%) and supports (α- and γ-Al_2O_3, ZrO_2, TiO_2, SiO_2), the turnover frequency for CH_4 consumption at 1023 K does not depend significantly on dispersion, indicating that CO_2 reforming at high temperatures is structure insensitive. No direct influence of the microstructure of the support on the reaction rates was detected. The effect of the support seems limited to the stabilization of the metal surface area, which is responsible for the activity of the catalyst [17].

Rh/Al_2O_3 promoted with V_2O_5 or TiO_2 were more active in the $CO_2 + CH_4$ reaction at 773 K than the unpromoted catalyst [59]. The increase of the conversion was attributed to the oxygen vacancies which formed on the promotors during the pretreatment of the catalysts. Vanadium oxide promotion enhances the activity of Rh/SiO_2 too and decreases the deactivation by carbon deposition [48]. This effect was attributed to the formation of VO_x overlayer on the Rh which thereby reduces the size of accessible ensembles of Rh atoms required for coke formation. The new sites at the Rh-VO_x interface were considered to be active for the dissociation of CO_2.

The activity and coke resistance of Rh/Al_2O_3 were enhanced by the addition of CeO_2. It was suggested that this effect is associated with the presence of two redox couples, which favors the activation of both CH_4 and CO_2 [60]. A Rh–CeO_2 interaction was induced by high temperature reduction, which resulted in the formation of oxygen vacancies in ceria. The electrons could transfer from Rh to CeO_2 on the perimeter. The Ce^{4+}/Ce^{3+} and $Rh^0/Rh^{\delta+}$ redox couples were found to coexist in Rh–CeO_2/Al_2O_3 catalyst. CH_4 decomposition on Rh released electrons, whereas CO_2 fill up the oxygen vacancies by accepting electrons. The Ce^{3+} species promote CO_2 dissociation into CO and surface oxygen, which reacts with CH_x to form CO [60].

Slow deactivation of 2% Rh/CeO_2 was observed at 1023 K during 70 h of the reaction, the methane conversion decreased from the initial value of 48.6 to 44.1%., which was attributed to catalyst sintering [61,62], the role in the deactivation of the coking was neglected.

Rh/ZSM-5 zeolite was found to be an active catalyst for dry reforming of methane, the reaction at 773 K was approaching the equilibrium product distribution, but adding 4–5% ethane to the reacting gas mixture lead to carbon deposition and to the deactivation of the catalyst [63].

Surprisingly, only a few studies reported on the effect of sulfur-containing compounds on the $CO_2 + CH_4$ reaction, although natural sources like natural gases and bio gases as possible candidates for being starting materials in this reaction, often contain more or less sulfur-containing compounds. Prichard et al. [64] did not observe any deactivation for 0.5% Rh/Al_2O_3 catalyst at 1068 K in the presence of 543 ppm dimethyl sulfide. In their opinion, this is caused by the high temperature, because at this temperature the interaction between the sulfur and the catalyst was limited.

The effect of H_2S (22 ppm) on the reaction of CO_2 with CH_4 at 773 K over TiO_2, SiO_2, Al_2O_3, ZrO_2, and CeO_2-supported Rh catalysts was examined [65] (Figure 3).

It was found that H_2S suppresses the formation of CO and H_2 in all cases, but on Rh/TiO_2 and on Rh/ZrO_2 the CO/H_2 ratio increased in time, indicating that H_2S poisons the secondary processes of the reaction to different extents. Therefore, the effect of H_2S on the CO_2 hydrogenation and the steam reforming of methane were investigated. It was found that the rate of methane formation in the $CO_2 + H_2$ reaction increased on TiO_2 and on CeO_2 supported metals (Ru, Rh, Pd), but on all other supported catalysts or when the H_2S content was higher than 22 ppm the reaction was poisoned [66]. The promotion effect of H_2S was explained by the formation of new centers at the metal–support interface.

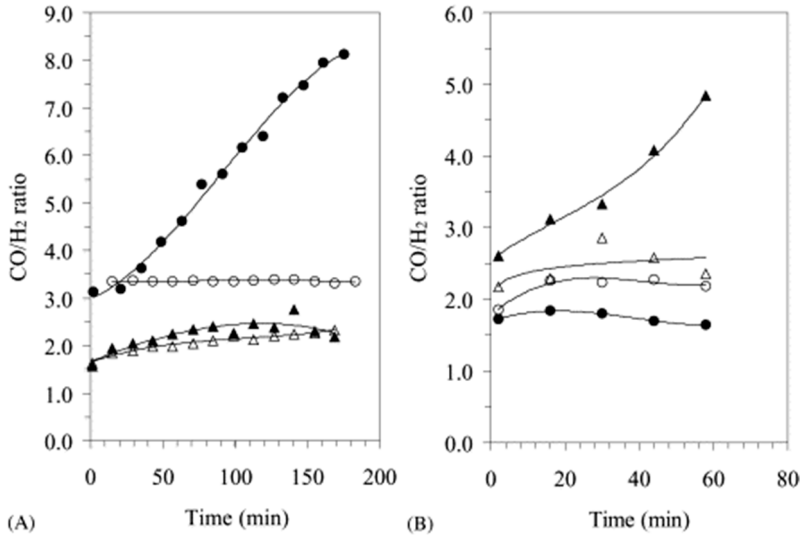

Figure 3. The CO/H_2 ratio formed in the $CO_2 + CH_4$ reaction at 773 K in the presence (solid symbol) and in the absence of H_2S (open symbol) on Rh/TiO_2 (○), Rh/SiO_2 (Δ) (**A**) and on Rh/Al_2O_3 (○), Rh/ZrO_2 (Δ) (**B**) catalysts. The flow rate of the reactants was 300 mL/min for Rh/TiO_2 and 80 mL/min for the other catalysts. (Reprinted with permission from [65]. Copyright Elsevier 2004).

Rh supported on La stabilized γ-Al_2O_3 has an outstanding catalytic activity for dry reforming of methane at 1073 K, but it was severely poisoned by even small amounts (below 1 ppmv) of sulfur in the feed [67]. The reverse water–gas shift reaction, occurring simultaneously with dry reforming, was only slightly affected by sulfur poisoning, approaching the equilibrium even at high S-levels. Sulfur inhibition was reversible and the Rh-catalyst slowly recovered its initial activity after the removal of sulfur from the feed.

4.2. Supported Ruthenium

Supported Ru catalyst is the best in some comparisons, while other studies show that it is one of the less active catalysts.

The support affected significantly the catalytic activity of supported Ru in the CO_2 reforming of methane at low temperature. With 0.5% Ru/La_2O_3 at 873 K CH_4 conversion reached 28.7% in stoichiometric CH_4 and CO_2 (1:1) mixture in a continuous flow reactor. On 0.5% Ru/Al_2O_3, it was only 5.7%. Y_2O_3 and ZrO_2 exhibited higher catalytic activities in this reaction (25–29%), but SiO_2 or TiO_2 gave lower conversions of CH_4 (less than 12%) [68].

On a turnover frequency basis, the activity decreased in the order of Ru/TiO_2 > Ru/Al_2O_3 >> Ru/C under conditions where heat and mass transfer limitations do not exist [69]. The catalytic activity under 0.1 MPa at 1023 K depends on the basicity of the supports ($Ru/MgO > Ru/Al_2O_3 > Ru/TiO_2 > Ru/SiO_2$) indicating that the CO_2 adsorption ability, the formation of carbonates on the supports determine the efficiency of the catalysts. Similar conclusion was reached on supported Rh catalysts [50]. Under 2 MPa pressure the activity correlated with the BET surface area, the activity order was $Ru/SiO_2 > Ru/Al_2O_3 > Ru/MgO > Ru/TiO_2$. On Ru/TiO_2 carbon deposition was not observed, the lowest activity of this catalyst was attributed to the SMSI effect [70].

Comparing the activity of Ru/Al_2O_3, Ru/SiO_2, and Ru/graphite [71] at 823 K it was found that at the beginning of the reaction the alumina supported catalyst has the highest activity, but it decreased continuously. The graphite-supported sample exhibits a rather stable activity, in contrast with the oxide-supported catalysts. The fastest deactivation rate is observed for Ru/SiO_2, its activity decays dramatically during the first 5 h. For the explanation of this observation, it was supposed that the activation of both reactants takes place on the metal surface and the accumulation of carbon species formed from CH_4 decomposition on the metal finally hinders CO_2 dissociation and results in a rapid deactivation of this catalyst [72]. The outstanding activity of Ru/TiO_2 compared to Ru/Al_2O_3

or Ru/C was attributed to the presence of interfacial Ru-Ti^{n+}-O_x species which markedly enhanced the activation of the reactants.

Several research groups investigated the activity of Ru/Al_2O_3 in the CO_2 + CH_4 reaction and obtained quite different results [17,18,25,31,62,69]. Direct comparison of the catalytic activities published in different papers is difficult due to the different reaction conditions used. Bradford and Vannice [69] extrapolated the results of each author to the same conditions using kinetic equations and it was found that there are two magnitude differences between the calculated turnover frequencies. These values correlate with the space velocity, the lower the space velocity the lower the TOF value. This observation was explained by the fact that the space velocity, the residence time influence reverse and secondary reactions and these result in differences in TOF values. The other possibility of the great differences in the turnover number is the effect of chlorine. Most of the catalysts were prepared using $RuCl_3$ and Cl could be detected with XPS on the surface. The Ru/Al_2O_3 catalyst with the lowest TOF value was prepared with $Ru_3(CO)_{12}$ [25]. Finally, it was concluded that it seems possible that Cl could promote the dry reforming of methane over supported Ru by facilitating CH_4 activation [69]. The particle size also influenced the activity of Ru. Silica supported Ru with lower Ru loading performs a better activity in comparison to the sample with higher Ru content [73].

Ru/NaY activity was higher than that of Ru/SiO_2, but unlike Ru/SiO_2 did not deactivate during the reaction, since the charge compensation protons caused dealumination accompanied by the local destruction of the zeolite structure [74].

Three percent Ru/Al_2O_3 exhibited good stability during the 70 h exposure to undiluted equimolar CH_4/CO_2 gas stream at 1023 K but the deactivation of the catalyst was observed during temperature programmed activity tests in the examined range of operating conditions, which was caused by metallic cluster sintering. A general trend was observed, namely that increasing CH_4/CO_2 ratio in the feed stream positively influenced carbon deposition, which revealed CH_4 as the primary carbon source [62].

The catalytic activities of 5 wt% Ru supported on alumina, ceria, and ceria/alumina with different proportions of ceria were studied for the methane reforming reaction with CO_2 in the temperature range of 673–1073 K. Ru/Al_2O_3 was a stable catalyst presenting no coke deposition. The addition of ceria on alumina can enhance the activity of ruthenium-based catalyst by the presence of Ru–Ce interaction [75].

2% Ru supported on Mg and/or Al oxides including γ-Al_2O_3, $MgAl_2O4$, $Mg_3(Al)O$ (prepared from Mg-Al layered double hydroxide), and MgO showed great differences in the catalytic performance for the CH_4 + CO_2 reaction [76]. The activities of Ru/MgO and $Ru/Mg_3(Al)O$ were higher than those of $Ru/MgAl_2O_4$ and Ru/γ-Al_2O_3, which might be related to the strong base intensity of the support and to the more accessible surface Ru^0 atoms, respectively. In a catalytic test at 1023 K for 30 h, $Ru/Mg_3(Al)O$ showed excellent stability, while a significant deactivation was observed on Ru/γ-Al_2O_3, $Ru/MgAl_2O_4$, and Ru/MgO. It was demonstrated that the sintering of Ru particles was mainly responsible for the catalyst deactivation.

In contrast with it, it was found that the activity of 4% $Ru/MgAl_2O_4$ in the 723–1023 K temperature range was stable in the CO_2 + CH_4 reaction, although the carbon dioxide and methane ratio was 3:1 [77]. The Ru particle size was found to remain stable during repeated methane reforming experiments, thus preserving the nanostructure.

A 0.15% $Ru/MgAl_2O_4$ catalyst prepared by physical vapor deposition method exhibits 1 or 2 orders of magnitude higher activity than Ru catalysts prepared by incipient wetness impregnation [78]. This sample, instead of deactivation or coke deposition, demonstratec an activity increase of 1.5 times after reaction at 1123 K for 600 h. Ru initially was dispersed as isolated atoms on the support, then condensed into clusters (1.1 nm), and finally retained as faceted nanoparticles (2.7 nm) during the reaction, becoming more and more active by decreasing the barrier of breaking the C−H bond of methane.

Ru/La_2O_3 catalyst remained stable for more than 80 h in the 823–903 K temperature range when the CO_2/CH_4 ratio was equal to unity. However, a significant deactivation

was observed at 823 K when the reaction was carried out in CO_2 rich stream. It was demonstrated by XPS that the partial re-oxidation of metallic Ru could be one of the factors that produces the catalyst deactivation [79]. In the case of Ru supported Al_2O_3 promoted with different oxides negative temperature dependence was observed, which was explained by the loss of structure of the solids and complete oxidation of ruthenium species at the reaction temperature [80].

Substitution of just 0.5 atom% of Ru in La_2O_3 ($La_{1.99}Ru_{0.01}O_3$) enhanced the conversion by 20 times when compared to the activity exhibited by La_2O_3 [81]. The oxygen storage capacity of the Ru doped sample was considerably higher than that of clean La_2O_3, which resulted in higher conversions of CH_4 and CO_2. When the Ru concentration was higher (1 atom% $La_{1.98}Ru_{0.02}O_3$), the activity decreased considerably, indicating the role of the ionic nature of substituted Ru at low dopant concentrations. DRIFTS studies demonstrated the role of a specific type of carbonates in promoting the activity of the catalyst [81].

It was shown that a very small amount of Ru (0.13 wt%) supported on ZrO_2-SiO_2 is very active and stable for the dry reforming of methane and the coke formation was suppressed at 1073 K while Ru/SiO_2 and ZrO_2-SiO_2 showed poor activity. When Ru was deposited at the SiO_2, Ru particle size was relatively large at 6.3 nm, but the Ru particles significantly decreased to 1.4 nm when Ru was deposited at the ZrO_2-SiO_2 support [82].

4.3. Supported Platinum

The reaction of CH_4 + CO_2 on Pt wire up to 1373 K produced mainly CO even at a CH_4/CO_2 ratio of 4.3, but if coke is also present on the Pt the dominant reaction becomes the pyrolysis of CH_4 to form C_2H_2 and C_6H_6 [83].

The activities of different supported Pt catalysts were initially similar at 875 K [84,85]. However, the Pt/γ-Al_2O_3 deactivated almost completely in the first 10 h of the reaction. Pt/TiO_2 lost 80% of its activity within 50 h, whereas the Pt/ZrO_2 showed only a 5% deactivation within 50 h on stream [84]. For all catalysts, the decrease in activity is caused by carbon formation, which blocks the active metal sites for reaction since the carbon formation rate decreased in the order Pt/γ-Al_2O_3 >> Pt/TiO_2 > Pt/ZrO_2 [85]. Evidences were presented that deactivation is caused by carbon formed on the metal and it is associated with overgrowth of the catalytic active perimeter between the support and the metal. Bradford and Vannice [86] also found that Pt/ZrO_2 and Pt/TiO_2 exhibited high stability even after 80 to 100 h on-stream although the Pt/SiO_2 and Pt/Cr_2O_3 catalysts deactivated significantly. The differences in the stability of the catalysts were explained in the case of Pt/SiO_2 and Pt/Cr_2O_3 by the apparent absence of any remarkable metal–support interaction which resulted in significant carbon deposition and so rapid deactivation. Pt on TiO_2 suppresses the carbon deposition, due to an ensemble effect of TiO_x species migrating onto the Pt surface. The low carbon deposition on Pt/ZrO_2 was explained by an interaction of Pt with Zr^{n+} centers, the participation of lattice oxygen species at the metal–support interface, or by the partial coverage of Pt by ZrO_xspecies, as occurs with titania [86]. The same activity order was found by van Keulen et al. [36] and they interpreted the results in similar way, but the lower carbon deposit on Pt/ZrO_2 was explained that the carbon formed on the catalyst is gasified by reaction with CO_2.

The TOF value of CO_2 consumption at 925 K for Pt/ZrO_2, Pt/TiO_2, and Pt/γ-Al_2O_3 was two orders of magnitude higher compared to Pt-black or Pt/SiO_2 [87]. From these observations it was concluded that in supported Pt catalysts not all the surface Pt atoms contribute equally to the activity of the catalyst; Pt atoms on the support–metal perimeter determine the activity. This can be explained by the fact that the CO_2 activation occurs via carbonate species on the support that must be in the surroundings of the Pt particles to react with the methane which is activated on the Pt.

The catalytic efficiency of Pt/ZrO_2 in the CO_2 + CH_4 reaction was studied by different research groups [36,87–94]. It was observed that on Pt/ZrO_2 both CH_4 and CO_2 dissociate independently of each other in the CO_2 + CH_4 reaction [94]. The dissociation of carbon dioxide produces oxygen, while the decomposition products of methane react

with the oxygen. When there is a large quantity of oxygen on the surface, the CH_4 can be oxidized to CO_2. CO_2 dissociation and its reverse reaction is also effected by the amount of surface oxygen

$$CO_{2ads} \rightleftharpoons CO_{ads} + O_{ads}. \quad (8)$$

The activity and stability of Pt/Al_2O_3 and Pt/ZrO_2 was compared in different papers [89,90,95–97]. The activity decrease for Pt/Al_2O_3 was rather slow and minor above 1070 K, while it was fast and almost complete at low temperature (< 875 K) [89,95]. Others found that Pt/Al_2O_3 deactivated significantly at 1073 K (deactivation rate was 4%/h) [90,97]. The cause of deactivation on Pt/Al_2O_3 was attributed to coke deposition on Pt. On the other hand, coke hardly deposits on Pt/ZrO_2 which resulted in the high stability of this sample. It was found that the reactivity of coke on Pt with hydrogen was higher on Pt/Al_2O_3 than on Pt/ZrO_2 but the reactivity of carbon with CO_2 was the opposite. These results and the observation that the methane decomposition is slower on Pt/ZrO_2 than on Pt/Al_2O_3, resulted in the small carbon deposition on Pt/ZrO_2 under reaction conditions [96]. The main difference between the two samples was found in the CO_2 dissociation. On Pt/Al_2O_3 this step was assisted by hydrogen, while on Pt/ZrO_2 the dissociation takes place over the support involving the oxygen vacancies.

The reduction of carbon deposition over zirconia-alumina catalyst was related to Pt-Zr^{n+} interactions and to the high oxygen mobility on zirconia [90,97].

Ballarini et al. [93] also found that Pt/Al_2O_3 lost its activity at 1073 K due to the carbon deposition. Na or K addition to the catalyst enhances the stability since they provide basic sites, which promote the dissociation reaction of CO_2 into CO and O, and the O species can react with the surface carbon deposited on the Pt, thus cleaning the metallic phase of the catalysts. A similar effect can be achieved if at least 1% of CeO_2 is added to the Pt/Al_2O_3 catalyst [98] since CeO_2 promote the gasification of coke deposition, because the dispersity and thus the metal–support interfacial region will be higher.

Comparing the activity of Pt/ZrO_2 and Pt/SiO_2 it was found that the Pt/ZrO_2 was the best sample due to the ability of ZrO_2 to promote the CO_2 dissociation [99] which aids in the removal of carbon deposit from the metal. High reforming activity (CO_2 conversion was 96.4% at 1073 K) was observed for the $Pt/ZrO_2/SiO_2$ (4:1) sample among all the prepared ZrO_2/SiO_2 mixed oxides with different ratios (2:1 to 4:1) supported Pt [91]. The better catalytic properties of the $Pt/ZrO_2/SiO_2$ (4:1) were explained by higher Pt dispersion due to the absence of remaining free silica and the presence of higher amount amorphous $ZrSiO_4$.

The dry reforming of methane was compared on different alumina supported Pt catalysts [100]. It was observed that the morphological differences between the supports affect in general the catalyst performance. Pt is present as Pt^0 on all catalysts, but the dispersion and stability was higher on Pt supported on a nanofibrous alumina, which presents a better behavior in terms of reactivity. It was found that CO_2 activation is promoted by the CH_X species, which probably initiates the reforming reaction.

Deactivation of Pt/Al_2O_3 was prevented by the addition of Pr-, Zr-, or Nb-doped CeO_2 to the Pt/Al_2O_3 catalyst [101]. The presence of dopants decreased the carbon accumulation on Pt surface. It was stated that during the reduction of the catalysts the Ce^{4+}/Ce^{3+} ratio decreased on the surface—which was more significant for $Pt/CePr/Al_2O_3$—this resulted in the increase of oxygen storage/release capacity, which promotes the carbon removal from metallic surface.

High conversions and close to equal H_2/CO ratios were observed in the dry reforming of methane on 4% Ru/TiO_2 and 4% Pt/TiO_2 but on the Pt-Ru/TiO_2 bimetallic samples these values were lower than on monometallic catalysts [102]. Interestingly, the H_2/CO ratio for bimetallic catalysts decreased with increasing Pt content under the same conditions; for 3% Pt1% Ru/TiO_2 this ratio was below 0.2, while for Pt/TiO_2 it was found above 0.8.

4.4. Supported Palladium and Iridium

Nakagawa et al. [103] ranked the activity of the supported Ir catalysts as follows: $TiO_2 \geq ZrO_2 \geq Y_2O_3 > La_2O_3 > MgO \geq Al_2O_3 > SiO_2$. Carbon deposition was observed only on Al_2O_3 and SiO_2 supported catalysts and this resulted in the low stability of the catalysts. The effect of the support was attributed to the activation of CO_2 on the metal oxides. Similar order was observed on 5% Ir supported on TiO_2, MgO, Al_2O_3, and SiO_2 when the turnover rate for H_2 formation was compared at 773 K [104]. In these cases, a significant amount of carbon formation on SiO_2 (C/Ir_{surf} = 1.95) and MgO (C/Ir_{surf} = 1.08) supported catalysts was observed after 1 h of reaction at 773 K, on Ir/Al_2O_3 and Ir/TiO_2 only traces of carbon were detected ($C/Ir_{surf} \leq 0.1$).

On Ir/Al_2O_3 doped with both alkaline (Na and K) and alkaline earth metals (Ba, Ca and Mg) of different concentrations (1, 5 and 10 wt%) was studied the dry reforming of methane [105]. The catalytic performance was affected by acid–base functions of the support that modify the metal–support interaction. It was found that the higher the dopant concentration, the better the performance. The highest activity was obtained for 1% Ir/Al_2O_3-10% Mg catalyst.

The turnover rate for CH_4 consumption in the $CH_4 + CO_2$ reaction increase linearly with increasing CH_4 pressure at 873 K on 0.8 wt% Ir/ZrO_2, but it were not influenced by CO_2 concentration [106]. These results indicate that Ir surfaces remain essentially uncovered by CH_4-derived intermediates or by reaction products, because co-reactant or product concentrations would have otherwise influenced the forward rates. CH_4 consumption rates increased with increasing Ir dispersion, as it varied with metal content (0.2–1.6 wt%) or support (ZrO_2 or Al_2O_3). These data contradict with the results of Mark and Maier [17] since they observed that there is no effect of catalyst particle size on the methane conversion at 1073 K in the case of 1% Ir/Al_2O_3 catalyst.

Long-term experiments show the excellent stability of the $Ir/Ce_{0.9}Gd_{0.1}O_{2-x}$ catalyst [107]. Carbon formation was totally inhibited or very limited under the most severe conditions of the study (1073 K, CH_4/CO_2 = 2).

$Ir/Ce_{0.9}Pr_{0.1}O_2$ catalysts prepared by different methods were also stable at 1023 K in the dry reforming reaction [108]. The highest activity of the sample synthesized by deposition–precipitation method was associated with the more enhanced basicity of the support, the more accessible Ir nanoparticles to transform CH_4 and the Ir-support boundary to remove the coke precursors.

The support significantly influenced the rate of the $CO_2 + CH_4$ reaction on the palladium catalyst. The specific activities of Pd/TiO_2 exceeded by almost one order of magnitude the TOF value for CO formation of the less active Pd/Al_2O_3 and Pd/SiO_2, and it was more than twenty times higher than on Pd/MgO [109]. It was suggested that the activity order of the Pd catalysts may be related to their efficiency in the dissociation of CO_2, where the same sequence of activity was found. It could mean that on supported palladium, the activation of carbon dioxide should play an important role in the $CH_4 + CO_2$ reaction. The high activity of Pd/TiO_2 may be associated with the extended electronic interaction between Pd and n-type TiO_2. The oxygen vacancy present on Pd titania interface could also promote the dissociation of carbon dioxide [109].

Pd/Al_2O_3 shows high initial activity but poor stability in the $CO_2 + CH_4$ reaction at 973 K due to Pd sintering and to a large amount of carbon deposition. Of the various promoters added to the catalyst (K, Ca, Y, Mn, and Cu), Y or Ca slightly increased the initial conversions, which can be attributed to the moderate reducibility of Pd species and to the increased Pd dispersion. In contrast, while the addition of K, Mn and Cu similarly reduced the reducibility of Pd species, the metal dispersions decreased owing to decoration effect or alloy formation [110]. Y-modified Pd/Al_2O_3 showed the best stability without activity loss in 20 h of reaction. This is probably because the addition of Y to the catalyst suppresses carbon formation and metal sintering and maintains Pd particle size below 10 nm. This particle size is crucial, below which carbon formation can be completely avoided under the reforming conditions.

A 0.86% Pd/CeO_2 catalyst showed activity in the dry reforming already at 623 K due to the presence of highly dispersed and very small Pd-nanoparticles (~2.9 nm), to metal–support interactions, and to the redox property of the support CeO_2 [111]. The high reducibility of CeO_2 (~32.8% Ce^{3+}) influenced methane activation at as low as 623 K. Only a slight decrease in conversion was observed due to sintering, re-oxidation and hydroxylation of the active Pd-nanoparticles at 1073 K during 12 h of reaction. The promoting effect of Ce^{3+} was also observed when the activity of 1% Pd/$MgO_{1-x}Ce_x^{3+}O$ was found to be greater than that of 1% Pd/$MgO_{1-x}Ce_x^{4+}O$ in the reaction at 1173 K [112]. This effect was attributed to the smaller size of Ce^{4+}.

5. Adsorption, Dissociation, and Activation of CO_2 on Noble Metals and on Supported Noble Metal Catalysts

It is known that CO_2 adsorbs on the surface of oxides used as catalyst support with the exception of some acidic oxides such as SiO_2. Spectroscopic analyses show that a variety of surface species can be formed, depending on the basicity of the surface, forming mixture of bidentate, monodentate, bridged carbonates, and bicarbonates [26]. In some cases, formate species were also detected after CO_2 adsorption. These observations indicate that hydrogen remained on the catalyst surface after reduction [26,113].

Any reaction of CO_2 requires its activation on the surface of the catalyst. There are different possibilities and therefore there are different theories for CO_2 activation on noble metals and on supported metal catalysts.

CO_2 could dissociate on metal surfaces to produce CO and adsorbed oxygen [114,115].

The reduction reaction could proceed via the formation of carbonate or formate species on the basic catalytic sites of the support [55].

The activation of CO_2 could occur on the interfacial sites of the catalysts, on the oxygen vacancies formed on the metal–oxide interface [49,88].

Another possibility for the activation of CO_2 is that the hydrogen formed in the decomposition of methane could promote the dissociation of CO_2, the formation of CO.

The adsorption and activation of CO_2 on clean noble metals has also been widely investigated [116,117]. It is generally accepted that CO_2 adsorbs weakly and molecularly on carefully cleaned noble metals at 100–300 K. In the case of Rh, there was a controversy concerning the nature of the interaction and particularly the dissociation of CO_2 on clean Rh surfaces. In the early studies, it was found that the adsorption of CO_2 is weak and associative on Rh metal [118]. The Somorjai group [119,120] reported that CO_2 dissociate on a Rh foil and on Rh single crystals, but Weinberg [121] and Goodman [122], on the basis of thermodynamic and kinetic results, indicated that the CO_2 sticking probability under the experimental conditions used would be by orders of magnitude smaller than needed to observe dissociation. It was demonstrated by field electron microscopy that the crystal structure of the Rh tip influenced the adsorption and dissociation of CO_2 [115], it was the fastest on {012} facets [114]. On Pt powder already at 293 K adsorbed CO was detected by DRIFTS indicating that CO_2 dissociation occurs [123].

Completely different results were obtained, when potassium or sodium adatoms, an electron donating promoter was deposited on Rh [124], Pt [125], Ru [126], and Pd [127]. After the low temperature (~100 K) CO_2 adsorption CO_2^- formed and it dissociates even at 150–200 K or can be transformed into carbonate-like species and CO, at a higher temperature.

The CO band appeared on the infrared spectra during CO_2 adsorption, or the metal is oxidized indicating the dissociation of CO_2 on supported noble metals on Rh [128], Pt [86], Ir [104], Ru [72,79], and Pd [109]. The preparation, in some cases the reduction temperature of the catalysts, the dispersity or the particle size of metal, the nature of the support, the adsorption temperature, and the CO_2 pressure all have an influence on this process.

The high temperature dissociation of CO_2 occurred on reduced alumina supported noble metals. The extent of CO_2 dissociation (the amount of CO formed related to the number of surface metal atoms) at 773 K was the largest for Ru and Rh, and the smallest for Pt and Ir [18]. On oxidized surfaces, dissociation of CO_2 was not observed. Not everyone

has detected CO bands after or during CO_2 adsorption, that is, the dissociation of CO_2 on supported noble metals [129]. Adsorption of CO_2 on Ru/TiO_2 formation of formate occurs and carbonate species associated with the support but CO not up to 723 K whereas in the presence of H_2 part of these species is converted to Ru-bonded carbonyls via the reverse water–gas shift reaction at the metal–support interface [113].

$$CO_{2(TiO_2)} + H_{(Ru)} \rightarrow (COOH)_{Ru-TiO_2} \rightarrow CO_{Ru} + OH_{TiO_2} \quad (9)$$

On Ru/SiO_2 linearly (2039 cm^{-1}) and bridge (1941 cm^{-1}) bonded CO, on Ru/Al_2O_3 only Ru-CO (2029 cm^{-1}) were detected by IR spectroscopy after CO_2 adsorption at 823 K [72]. On the IR spectra registered after CO_2 adsorption at 723 K on Pt/TiO_2, Pt/ZrO_2, Pt/Cr_2O_3, and Pt/SiO_2 bands characteristic for adsorbed CO (2060–2070 cm^{-1} and 1860–1894 cm^{-1}) were detectable indicating the CO_2 dissociation [86], but the nondissociative adsorption of CO_2 was also observed.

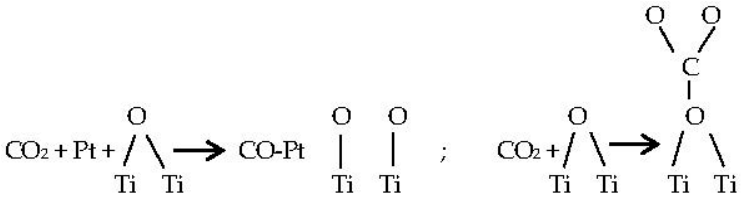

(10)

The dissociation of CO_2 on Rh/TiO_2 depends on the reduction temperature, the higher the reduction temperature the greater the CO formation [130]. These observations were explained by the speculation that oxygen vacancies produced by the reduction of the catalysts promote the dissociation of CO_2. A similar explanation was given for the dissociation of CO_2 in the case of vanadia promoted Rh/SiO_2 [48], vanadia or titania promoted Rh/Al_2O_3 [59] and Pt/ZrO_2 [96]. The active participation of the support in CO_2 dissociation was suggested in the case of CeO_2 supported noble metals [131]. It was found that by increasing the reduction temperature, the reduction of the CeO_2 increased, and the amount of CO desorbed after CO_2 adsorption also increased. The CO_2 could be activated on Ce^{3+} sites with the formation of CO and Ce^{4+} [73,131].

$$M\text{-}CeO_{2-x} + x\ CO_2 \rightarrow M\text{-}CeO_2 + x\ CO \quad (11)$$

CO_2 activation was related to the carbonate type species formed on the support [49,87]. On Pt/Al_2O_3 bicarbonates while on Pt/ZrO_2 bidentate carbonates were detected and the formation of latter species leads to easier activation of CO_2 than that of bicarbonates [95]. On Pt/SiO_2 did not form carbonate and on this sample CO was not detected after adsorption of CO_2 at 775 K [87].

At room temperature, CO_2 adsorbs on 1% $Pt/10\%ZrO_2/Al_2O_3$, the peaks at 1646, 1444, and 1228 cm^{-1} can be assigned to bidentate carbonate. While temperature increases, these species are activated and migrate to metal particles, being adsorbed as CO absorbing at about 2052 cm^{-1} (Figure 4). Thus, CO_2 activation on zirconia catalysts involves support and interfacial sites [90]. This conclusion support the finding that CO_2 dissociate on $PtZrO_2$ at 775 K but adsorbed oxygen or Pt-O was not detectable by EXAFS. It was concluded that the oxygen is consumed by the support at the metal–support interface [49].

The presence of oxygen vacancies in the bulk will be an additional driving force for the reduction of CO_2.

XPS measurements show that the CO_2 oxidized Rh at 398 K on Rh/Al_2O_3 during the dissociative adsorption [132]

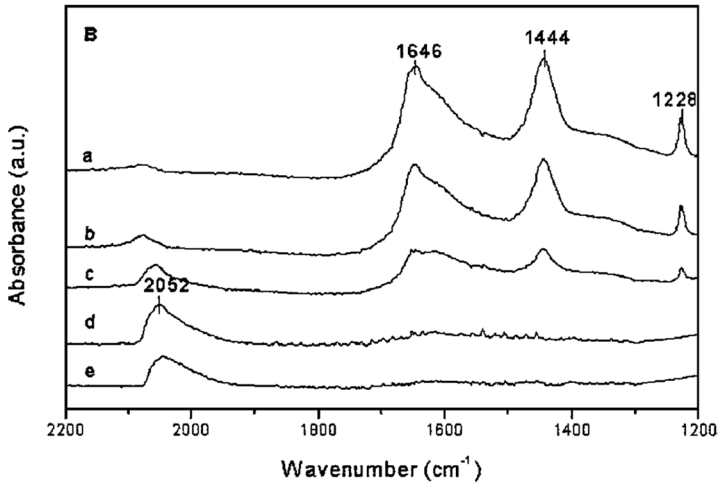

Figure 4. Thermal desorption IR spectra of adsorbed CO_2 for 1% Pt/10%ZrO_2/Al_2O_3 catalysts reduced at 773 K, with spectra obtained at the following desorption temperatures: (**a**) 298 K, (**b**) 323 K, (**c**) 373 K, (**d**) 473 K, and (**e**) 573 K. (Reprinted with permission from [90]. Copyright Elsevier 2001).

After the catalytic reaction at 903 K on Ru/La_2O_3 Ru^0 and Ru^{3+} species were observed by XPS [79]. The oxidation of Ru supported on La_2O_3 by CO_2 was also found by Matsui et al. [68]. Pulsed reaction with $^{13}CO_2$ indicates that Ru could be oxidized to give ^{13}CO; they proposed explaining this process by the following reaction step:

$$Ru/La_2O_3 + {}^{13}CO_2(ad) \rightarrow {}^{13}CO(gas) + Ru\text{-}O_x/La_2O_3. \quad (12)$$

The direct participation of La_2O_3 was suggested in the CO formation from CO_2 in the case of La_2O_3 supported noble metals or La_2O_3 doped catalysts. The carbon dioxide rapidly reacts with La_2O_3 to generate oxycarbonate, which reacts slowly with carbon formed in the methane decomposition (Equation (3)) to generate CO [38,79,133,134].

$$CO_2 + La_2O_3 \rightleftharpoons La_2O_2CO_3 \quad (13)$$

$$La_2O_2CO_3 + C\text{-}S \rightarrow La_2O_3 + 2\,CO + S \quad \text{(slow step)} \quad (14)$$

In addition to the CO_2 dissociation induced by an oxygen vacancy on Pt/ZrO_2, O'Connor et al. [96] did not rule out the CO_2 dissociation through carbonate formation.

$$CO_2 + \square_{Zr} \rightarrow CO^* + O_{Zr} \quad (15)$$

$$CO_2\,|_{Zr} + OH_{Zr} \rightarrow HCO_3\,|_{Zr} \quad (16)$$

$$HCO_3\,|_{Zr} + \square_{Zr} + * \rightarrow CO^* + OH_{Zr} + O_{Zr} \quad (17)$$

$\square_{Zr}$ means an oxygen vacancy at the zirconia surface and O_{Zr} is an surface oxygen species. It is most likely that these species are located at the Pt/zirconia interface.

Non dissociative adsorption of CO_2 during reaction occurs on the support, in the form of carbonates, as proved by FTIR of CO_2. Souza et al. [90] used in situ DRIFT experiments to prove that very weakly adsorbed carbonate species are formed, once the lattice oxygen of zirconia has been replenished by CO_2 which could decompose to CO.

$$2\,CO_2 + 2\,z \rightarrow CO_3^{2-} - z + CO - z \quad (18)$$

$$CO_3^{2-} - z + 2\,z \rightleftharpoons CO - z + 2\,O - z \quad (19)$$

$$CO - z \rightarrow CO + z \quad \text{(where z is a support site)} \quad (20)$$

The role of CO_2 is frequently assumed to be only a source of oxygen to the support.

6. Interaction of Methane with the Noble Metals and Supported Noble Metal Catalysts

The earlier results of the adsorption and dissociation of CH_4 on metal films were summarized by Frennet [135]. The theoretical calculations also show that the noble metals are active in methane dissociation [136]. It was found that the dissociation enthalpy of CH_4 is an important factor determining the catalytic activity of the metal. According to the trend in the calculated enthalpies, the most efficient catalysts for methane dissociation were Rh, Ru, and Ir are more active than Pd and Pt. These results are in agreement with experimental observations. Methane activation studies on single crystal surfaces have shown that the activation of C-H bonds depends sensitively not only on the metals but also on surface structure; specifically, surface steps and kinks are much more active than atoms on close-packed surfaces [137].

The dissociation, the activation of methane and its interaction with the catalyst have been studied separately on various supported noble metal catalysts. Treating Pt/SiO_2 [138] or different noble metals [39] with methane the dissociation of it was observed above 473 K, hydrogen and surprisingly ethane were formed. However, the activity of the catalysts quickly dropped to a low value, and after 15–25 min only traces of H_2 and C_2H_6 were detected. This suggests an accumulation of carbon deposit on the catalysts during this process poisoning the reaction. The rate of the ethane evolution passed through a maximum. The amount of hydrogen greatly exceeded that of ethane on all catalyst samples. The most active sample was Rh, but the largest amount of ethane was measured on Pt/SiO_2 [139]. The formation of ethane has been explained by the dissociation of methane on the surface and the resulting methyl group could dimerize to ethane and could decompose further to produce carbonaceous deposit.

$$CH_4(g) \rightleftharpoons CH_3(a) + H(a) \quad (21)$$

$$2\,CH_3(a) \rightleftharpoons C_2H_6(g) \quad (22)$$

The support influenced the hydrogen and ethane formation in the decomposition of methane. The most effective catalyst in the hydrogen formation was Pd/TiO_2 [140], but among the Rh catalysts, the alumina supported sample was the best followed by Rh/TiO_2, Rh/SiO_2, and Rh/MgO [46]. The effect of the supports on the CH_4 dissociation was explained by the different crystal size of the catalysts and/or with the ease of the carbon migration from the metal to the support [46,140]. The highest C_2H_6 formation was observed in all cases on silica supported samples.

It is generally assumed that the CH_4 dissociation occurs on metallic sites but on Rh/Al_2O_3 and Rh/ZrO_2 it was found that the CH_4 activation on Rh^0 would be better conducted when RhO_x sites are also on the surface, probably via oxygen assisted dissociation [141].

As the Equation (21) shows CH_4 adsorbs reversibly on the surface of noble metals arriving at the equilibrium. This conclusion is supported by the results of steady state isotopic tracing kinetic analysis (SSITKA) which detected methane on the surface of Pd/ZrO_2 and $Pd/\gamma\text{-}Al_2O_3$ under reaction conditions [142]. It was found that the rate constant did not depend on the dispersity of Pd, but others reported that the CH_4 activation is structure sensitive [72,143], and influenced by metal dispersion of different noble metals [17,58,144–146]. A direct correlation was found between the Rh dispersion and the turnover rate of the reaction [142,143,146].

The question is whether the surface carbon produced at high temperature from methane decomposition contains any hydrogen or not? By in situ IR spectroscopy on supported Rh could not detect CH_x intermediates [46], and when the carbon was reacted with D_2 only CD_4 was formed [147]. Similar was observed on Ru/Al_2O_3 but on Ru/La_2O_3 CH_2D_2, on Ru/Y_2O_3 CH_3D, CH_2D_2, and CHD_3 were also detected [148].

Several manuscripts have concluded from the kinetic parameters of the reaction, from the dependence of the reaction rate on the particle size that methane dissociates on

the supported noble metals. The activation and dissociation of methane can take place not only directly on the metals but also on the adsorbed O species [136,141,149], which may be formed from the dissociation of CO_2 [18], furthermore the oxygen in the support oxide [8,134], or the surface OH groups [71] can also facilitate this process.

Pakhare et al. [8,134] found by means of CH_4 TPR that the lattice oxygen on the surface of Ru or Pt containing pyrochlors ($La_2Zr_2O_7$) help react with CH_4. The oxygen or OH group can promote the dissociation of CH_4 by reacting with the CH_x groups formed in the first step.

Bradford and Vannice [26] detected by IR spectroscopy $H_2C = O$ (at 1690 cm^{-1}) species formation after CH_4 adsorption on TiO_2 supported noble metals. In addition, change in the intensity of OH groups was observed and on Rh and on Pt adsorbed CO were identified.

7. Surface Species Formed in the Interaction and in the Reaction of CO_2 with CH_4 on Supported Noble Metals

Examination of the interaction of reactants and products formed in the reaction on the surface helps to understand the whole process.

DRIFT spectra registered during co-adsorption of CO_2 + CH_4 gas mixture on Pt powder at 293 K show a marked increase in the intensity of the absorption band characteristic for adsorbed CO compared to CO_2 adsorption alone, implying that CH_4 promotes the dissociation of CO_2 [123], as it was observed on supported Rh [25,46,48], Pd [109] and Ir [25,104]. When the temperature was raised the intensity of the CO band increased, and its position shifted to higher wavenumbers. The spectral feature of CO formed in the co-adsorption differed from that observed during the adsorption of gaseous CO. For example, in the case of supported Rh the doublet due to the twin structure ($Rh(CO)_2$) at 2096 and 2029 cm^{-1} [150] was missing and the other CO bands, characteristic for linear and bridge bonded CO, absorbed at lower frequencies. The promotion of the dissociation of carbon dioxide is attributed to the effect of hydrogen—as it was found in the interaction of CO_2 + H_2 mixture [128,151]—formed in the decomposition of methane.

After the adsorption of CO_2 + CH_4 gas mixture at room temperature on Al_2O_3 supported noble metals mainly hydrogen carbonate were found on the IR spectra bands (1650, 1443, 1348, and 1302 cm^{-1}) [59]. With increasing the adsorption temperature the intensities of these bands decreased and above 548 K a band characteristic for linearly bonded CO was detected (Figure 5) [59]. Above 673 K a band was observed at about 1589 cm^{-1} characteristic for the O–C–O vibration (ν_{ass}) of formate groups adsorbed on alumina [150]. On V_2O_5 or TiO_2 doped alumina supported Rh the CO band appeared at lower temperature (Figure 5).

Similar spectra were recorded during the reaction of CO_2 + CH_4 at 723 K [147] or at 773 K [152]. It was observed that the intensity of formate band increased continuously during the reaction. It is surprising to observe adsorbed CO and formate species on the surface well above their desorption temperature [57,152]. It means that the formation rate of these form is higher than their desorption, decomposition or further reaction rate. This is supported by the observation that flushing the DRIFT cell with He after the catalytic reaction all bands disappeared immediately from the spectra [55].

The linearly bonded CO formed in the reaction of CO_2 + CH_4 similarly as was shown in the low temperature interaction of CO_2 + CH_4 absorbs at lower frequencies (~2030–2020 cm^{-1}) than the CO formed after gaseous CO adsorption. This effect was attributed to Rh carbonyl hydride formation [128–130].

On Rh/La_2O_3 CO bands (at 2036 and 1825 cm^{-1}) and absorptions characteristic for different $La_2O_2CO_3$ (at 720, 842, 864, 1060 and 1550 cm^{-1}) were observed during the exposure of the reaction mixture onto the catalyst at and above 773 K [34]. $La_2O_2CO_3$ formation was detected in all cases when La_2O_3 supported catalysts were used [153].

In the presentation of the activity of the catalysts, it was often mentioned that the significant decrease in activity in time is caused by carbon deposition. There are several theoretical possibilities for the formation of carbon: Decomposition of methane (3), the Boudouard reaction (6), and the hydrogenation of CO (the reverse reaction of 7).

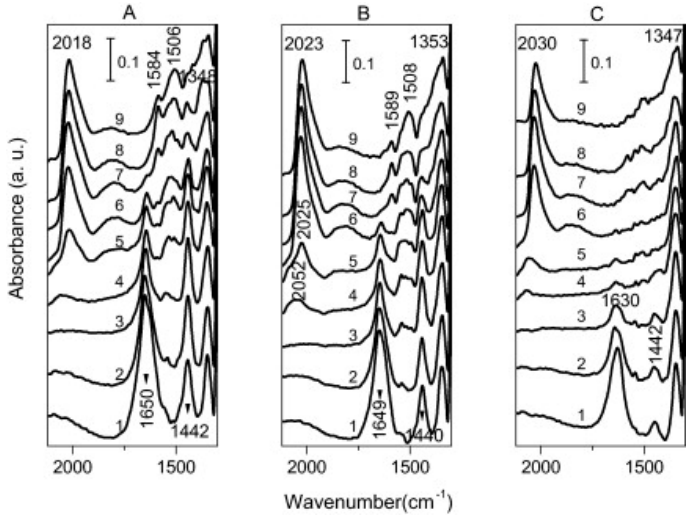

Figure 5. Infrared spectra recorded on Rh/Al_2O_3 (**A**), on Rh/TiO_2–Al_2O_3 (**B**) and on Rh/V_2O_5–Al_2O_3 (**C**) heated in the $CH_4 + CO_2$ gas mixture at 300 (1), 373 (2), 473 (3), 573 (4), 598 (5), 623 (6), 673 (7), 773 (8), 873 K (9). (Reprinted with permission from [59]. Copyright Elsevier 2011).

On theoretical calculation, it was found that with increasing the particle size increased the carbon formation. At low temperature CO was identified as the precursor for carbon, but CH_4 was found to be the main source of carbon at high temperature [154]. Transient isotopic experiments indicate [43,55,152,155] that on Rh/Al_2O_3 during the reforming reaction accumulated carbon is mainly derived from the CO_2 molecule, since after the $^{13}CH_4 + {}^{12}CO_2$ reaction on Rh/Al_2O_3 in the temperature programmed oxidation (TPO) mainly $^{12}CO_2$ was formed [44,55].

$$CO_2 + 2\,s \rightarrow CO\text{-}s + O\text{-}s \quad (23)$$

$$CO\text{-}s + s \rightleftharpoons C\text{-}s + O\text{-}s \quad (24)$$

where (s) is a site on the Rh surface or on the metal support interface.

In the case of Pt/ZrO_2 the main fraction of carbonaceous deposit was formed from the dissociation of CH_4 the preferred species was CH_2* [156].

Graphitic carbon was observed on the Pt/TiO_2 and Ru/TiO_2 [102] after the reaction by TEM but on $Pt/MgO\text{-}Al_2O_3$ [80], on Ru supported modified SiO_2 [73], on $Rh/\alpha\text{-}Al_2O_3\text{-}La_2O_3$ [38] filamentous carbon was found. According to experience the extent of carbon deposition on noble metals is usually lower than on Ni because carbon atoms can dissolve in Ni crystal and carbon fibers could form. This mechanism does not work on noble metals [157]. Raman spectra of the used $Pt/CeO_2\text{-}Al_2O_3$ and $Ru/MgO\text{-}Al_2O_3$ catalysts [80] especially after the reaction at 923 K, on Rh/La_2O_3 [153], on different Pd/Al_2O_3 [110], on $Pt/ZrO_2/SiO_2$ [91] show intense bands at 1580–1595 and 1339–1350 cm^{-1} which could assignation to the so called G and D band, respectively. The G band is related to the graphitic carbon and the D band to the disordered structure [80]. The detection of graphitic carbon by Raman spectroscopy was successful even when with TGA no carbon formation was detected [153].

The formation of graphitic carbon was detected on different Pd/Al_2O_3 [110], on Ru/SiO_2 [73] by using XRD spectroscopy.

Examination of the reactivity of the surface deposited carbon by temperature programmed hydrogenation (TPH) or oxidation as well as TEM images showed that carbon can occur in different forms on the surface, which can be transformed into each other depending on the temperature and the time elapsed since their formation. The reactivity of the surface carbon was almost the same regardless of whether it was formed either from the decomposition of CH_4 or from the disproportionation of CO or from the reaction of

CO_2 + CH_4. The gasification of surface carbon deposit is an important step enhancing the stability of the catalysts.

The reactivity of the surface carbon formed from CH_4 decomposition at 523 K, studied by TPH [46,63], exhibited practically the same features as those established for supported Rh catalysts following the dissociation of CO [57]. Three different carbon forms were distinguished: (i) The highly reactive form (α), which can be hydrogenated even below 350 K; (ii) a less reactive deposit (β), with T_{Max} = 500 K; and (iii) the relatively inactive form (γ), which reacts with hydrogen only above 650 K. Similar TPH spectra were registered on different $RhCu/Al_2O_3$ after decomposition of CH_4 at 623 K [158]. The reactivity of surface carbon, that is, the relative ratio of the three forms, is very sensitive to the temperature of its formation and also to the duration of its thermal treatment. Above 623 K, a significant aging was observed, with transformation of the more reactive form into less reactive ones. When decomposition of CH_4 occurs at 923 K a relatively inactive form of carbon was obtained (T_{Max} = 973 K), suggesting that aging of the carbon produced occurs [155].

$$C_\alpha\text{-s} \rightarrow C_\beta\text{-s} \rightarrow C_\gamma\text{-s} \quad (25)$$

These results supported by the observation that in the case of Ru/Al_2O_3 and Ru/La_2O_3 the TPH peak shifted to higher temperature as a function of the CH_4 decomposition temperature [148]. On Ru/Al_2O_3 there is a carbon form which did not react with H_2 up to 1073 K.

TPH for Pt/Al_2O_3 after exposure to CH_4 at 1070 K showed a peak above 873 K, while on Pt/ZrO_2 the CH_4 formation was observed above 1073 K. These indicate that some of the surface carbon on Pt/Al_2O_3 is more reactive with H_2 than on Pt/ZrO_2 [95], but some of the coke could not remove by H_2 even at 1273 K.

The TPH profiles of the used Ru/SiO_2 [73], or that of different noble metals supported on spinell [30] catalysts clearly showed the existence of two types of carbonaceous species on the catalysts. A first peak is observed at temperatures between 620 and 680 K on different catalysts depending on the metal. This peak is related to amorphous carbon located at the interior of the active metal particles. A second peak is observed at temperatures above 873 K, identified as whisker-like filamentous carbon. The THP of 0.5% Rh/Al_2O_3 used in the CO_2 + CH_4 reaction at 923 K for 10 min showed three well resolved peaks. The most reactive hydrogenated at low temperature (373 K), the most abundant reacted at 423–593 K, and the least active carbon form above this temperature [43,155].

The TPO profile of used noble metal catalysts supported on $MgAl_2O_4$ depends on the metals. Pt and Ir showed one peak in the temperature range of 573–700 K which was related to the oxidation of amorphous carbon. In addition to this form for the other samples a second peak was also detected; in the case of Pd it was found at higher temperature above 873 K, due to the formation of whisker carbon. On Ru and Rh supported on spinel a TPO peak was observed at about 373 K which could be related to (C_α) carbide like structure [30]. In contrast on Ru/SiO_2 TPO peak characteristic for whisker was observed and the carbide like species was missing [73].

After CO_2 + CH_4 reaction at 923 K four TPO peak were registered on 0.5% Rh/Al_2O_3, the T_{Max} were at 373, 453, 543, and 603 K [43] similarly to on 0.5% Rh/La_2O_3 [30]. Ghelamallah and Grangers found that on Rh/La_2O_3 the first TPO peak appeared below 523 K and it was assigned to carbon deposited on metal, the second (635–661 K) type of coke is on the metal support interface, and the third one (693–798 K) accumulated on the support, and the most inactive carbon (above 973 K) was identified as graphite [159].

TPO profiles of carbon deposited on Pt during the reaction at 1123 K showed a main peak at 893 K, which is typical for the oxidation of carbon with a nanotube structure. Only a small peak was observed between 613 and 623 K, attributed to oligomeric and polymeric carbon. This indicates that, regardless of the source of carbon (CH_4 or CO_2), the majority of the carbon species is present on the catalyst surface in the form of carbon nanotubes [156]. Similar TPO curves were found on different Pd/Al_2O_3 [110].

With increasing the reaction temperature on Ru substituted $La_2Zr_2O_7$ the amount of carbon deposit decreased although the TPO peaks shifted to higher temperature [8]. This means that the reactivity of deposited carbon decreases with increasing the reaction temperature.

On Rh/Al_2O_3 the carbon produced in CH_4 decomposition at 773 K react with oxygen above 400 K but up to 570 K small amount of CO_2 was detected. The main CO_2 peak was observed at 745 K [46].

The reactivity of surface carbon was investigated by temperature programmed reaction with CO_2 (the reverse Boudouard reaction (6)). On Rh/Al_2O_3 the carbon—produced at 773 K in the decomposition of CH_4—reacted with CO_2 above 550 K and the reaction proceeded at a higher rate above 700 K [46]. Similar results were obtained on Pt/Al_2O_3 [89,95] peak was observed below and above the reaction temperature and these were assigned to carbon on Pt and on Al_2O_3, respectively. For Pt/ZrO_2 also two peaks were registered but both react below reaction temperature and these were attributed to coke on Pt [89,95].

8. The Proposed Mechanism for the CO_2 + CH_4 Reaction on Supported Noble Metals Catalysts

In the previous chapters the adsorption, dissociation, and activation of CO_2 and CH_4 on supported noble metals were discussed, we presented the different experimental results and the processes proposed based on them. It means there is still some debate on the reaction mechanism of this reaction. Regarding the reaction mechanism for CO_2 + CH_4 reaction basically three different, but same in a few steps' reaction mechanisms were proposed. The first involves the adsorption of CH_4, the second the activation or dissociation of CO_2 and the third one when both component dissociate in the first step. Further differences between the reaction mechanisms are that the dissociation of CH_4 or CO_2 takes place directly or in some reaction, and that this process takes place on the metal, on the support, or at the interface.

The mechanisms of the reaction could be divided into two groups: Mono- and bifunctional mechanism. According to the monofunctional mechanism the activation of both CO_2 and CH_4 occurs on the metal sites, but in the latter cases the CO_2 is activated on the support or on the metal–support interface and the CH_4 on the metal.

A dissociative methane and carbon dioxide adsorption is proposed by Rostrup-Nielsen and Bak-Hansen [19] on different alumina stabilized magnesia supported noble metals

$$CH_4 + * = CH_3* \rightarrow CH_2* \rightarrow CH* = C \quad (26)$$

$$CO_2 + * = O* + CO \quad (27)$$

$$CH_x* + O* = CO + x/2\ H_2 + 2* \quad (28)$$

In the case of supported Rh and Pd catalyst, although the dissociation of CO_2 has been shown on these samples, it was suggested that during the reaction, the main route for CO formation is the hydrogen assisted CO_2 dissociation [46,109].

$$CH_4 = CH_{3(a)} + H_{(a)} \quad (29)$$

$$CO_2 + H_{(a)} = CO + OH_{(a)} \quad (30)$$

$$CH_4 + O_{(a)} = CH_{3(a)} + OH_{(a)} \quad (31)$$

$$CH_{3(a)} = CH_{2(a)} + H_{(a)} \quad (32)$$

$$CH_{2(a)} = CH_{(a)} + H_{(a)} \quad (33)$$

$$CH_{x(a)} = C + xH_{(a)} \quad (34)$$

$$CH_x + O_{(a)} = CO + xH_{(a)} \quad (35)$$

$$CH_{x(a)} + CO_2 = 2\ CO + xH_{(a)} \quad (36)$$

$$2\ H_{(a)} = H_{2(g)} \quad (37)$$

$$2\ OH_{(a)} = H_2O + O_{(a)}$$

In the case of Rh/Al_2O_3 the reverse Boudouard reaction (6) and the

$$C + H_2O = CO + H_2 \quad (38)$$

reaction was also confirmed [46].

Raskó and Solymosi showed that the adsorbed CH_3 radical and CO_2 react with each other at the metal–substrate interface on Rh/SiO_2. CH_3 groups adsorbed on the support migrate from the support to the metal [160].

Direct dissociation of CO_2 [55,71,149] and CO [55,149] and the further reaction of adsorbed oxygen, OH groups were not considered in former mechanism [55,58,149] and therefore it was completed by the following reactions:

$$CO_{2(a)} \rightarrow CO_{(a)} + O_{(a)} \quad (39)$$

$$CO_{(a)} \rightarrow C + O_{(a)} \quad (40)$$

$$O_{(a)} + H_{(a)} \rightarrow OH_{(a)} \quad (41)$$

$$CH_{(a)} + OH_{(a)} \rightleftharpoons CO_{(a)} + H_2 \quad (42)$$

$$C + OH_{(a)} \rightleftharpoons CO_{(a)} + H_{(a)}. \quad (43)$$

Mark and Maier [17] proposed a mechanism for the reaction on Rh/Al_2O_3 where the dissociative CH_4 adsorption is rate limiting step, followed by the direct reaction of CO_2 with adsorbed carbon. This reaction mechanism was also confirmed on Ru [147,161] and Ir catalysts [147].

Bifunctional mechanisms in which methane is activated on the metal and carbon dioxide on the support have been proposed for Pt metals dispersed on supports, such as ZrO_2 [49,86,87,90,94], TiO_2 [50,86], or Al_2O_3 [50,71].

The following bifunctional mechanism (where p is a platinum site and z a support site) was proposed by Souza et al. [90] for $CH_4 + CO_2$ reforming:

$$CH_4 + p \overset{k_{CH_4}}{\Leftrightarrow} CH_x{-}p + \left(\frac{4-x}{2}\right)H_2 \quad (44)$$

$$CO_2 + z \overset{K_{CO_2}}{\leftrightarrow} CO_2 - z \quad (45)$$

$$2\ CO_2 + 2\ z \rightarrow CO_3^{2-} - z + CO - z \quad (46)$$

$$CO_3^{2-} - z + 2\ z \quad \Leftrightarrow \quad CO - z + 2\ O - z \quad (47)$$

$$CO - z \rightarrow CO + z \quad (48)$$

$$H_2 + 2\ p \leftrightarrow 2\ H - p \quad (49)$$

$$CO_2 - z + 2\ H - p \leftrightarrow CO + H_2O \quad (50)$$

$$CO_2 - z + 2\ CH_x - p \overset{k}{\rightarrow} 2\ CO + \frac{x}{2}H_2 + z + p \quad (51)$$

The occurrence of the bifunctional mechanism is supported by the observation that when TiO_2, Al_2O_3, or MgO was mixed with the Rh/SiO_2 catalyst, the conversion increased significantly, but when mixed with SiO_2 it did not change [46]. This was explained by the fact that neither carbonates nor formate are formed on SiO_2 which forms may be responsible for the increase of reaction rate.

Bitter et al. found [49] that the activity of Pt/ZrO_2 increased linearly with increasing the Pt-ZrO_2 perimeter, since the carbonate on the interface is reduced by the CH_x species on the metal to form CO and formate. The formate species then decompose to CO and

OH and subsequently the OH groups can either be desorbed as water or react with CH_4 to form CO and H_2.

On La_2O_3 [34,38,68,79,86,134] supported catalysts it was suggested that the $La_2O_2CO_3$, formed in the adsorption of CO_2 (Equation (13)), react with the surface carbon (Equation (14)) formed in the decomposition of methane.

We have seen that in recent years, many ideas have been developed for the CO_2 + CH_4 reaction, but to date there is no clear explanation for what and why influences CO_2 dissociation, what kind of secondary reactions take place on the surface of noble metal catalysts.

9. Conclusions

This review summarizes the studies on the CO_2 + CH_4 reaction, the dry reforming of CH_4 on supported noble metal catalysts. Comparing the activity and stability of different supported metals, it was found that the best catalysts are among the noble metals, Rh and Ru. However, these metals are expensive and so to make the process uneconomical, but noble metals can be used to promote the cheaper Ni or Co catalyst which could help in removal of carbon deposit, thus increasing the stability of the catalyst.

Comparing the activity of noble metals and the effect of carriers, there are significant differences in the literature. The acidity, basicity and the reducibility of the supports basically influence the efficiency of the catalyst. The oxygen vacancies formed on the metal–support interface improve the activity as these sites promote CO_2 activation but the SMSI interaction reduces it. Alkaline or alkaline earth metal additive increases CO_2 dissociation and thus the efficiency of the catalysts

The possibility of the activation and dissociation of CO_2 and CH_4 on clean metals and on supported noble metals were discussed separately. There are different possibilities and therefore there are different theories for CO_2 dissociation or activation. CO_2 could dissociate on metal surfaces, this reaction could proceed via the formation of carbonate or formate species on the acidic or basic sites of the support, or on the metal–support interface. In the reaction the hydrogen assisted dissociation of CO_2 was also suggested. It is generally accepted that CH_4 decomposes primarily on the metal thus having appropriate dispersion of the metal is important. The activation and dissociation of methane can take place also on the surface O species. The main problem of the reaction is the carbon deposition and the reactivity of the surface coke. Surface carbon can be formed from methane while others suggest that the source of the surface carbon is CO_2. Carbon can occur in different forms on the surface, which can be transformed into each other depending on the temperature and the time elapsed since their formation. These processes are influenced by, among others, the metal, the metal particle size, the support and therefore significant differences have been found in the order of activity of the catalysts, the carbon deposition, and in the reactivity of surface carbon.

Basically, two reaction mechanisms were proposed, according to the mono-functional mechanism the activation of both CO_2 and CH_4 occurs on the metal sites because the support is completely inert. In the bi-functional mechanism the CO_2 is activated on the support or on the metal–support interface and the CH_4 on the metal and the reaction intermediates react on the interface.

Funding: This research received no external funding.

Data Availability Statement: The data presented in this study are available in the cited references.

Conflicts of Interest: The author declares no conflict of interest.

References

1. Earth System Research Laboratory Global Monitoring Division. Available online: https://www.esrl.noaa.gov/gmd/ccgg/trends/ (accessed on 17 December 2020).
2. National Aeronautics and Space Administration Goddard Institute for Space Studies. Available online: https://data.giss.nasa.gov/gistemp/graphs/ (accessed on 17 December 2020).

3. York, A.P.E.; Xiao, T.-C.; Green, M.L.H.; Claridge, J.B. Methane Oxyforming for Synthesis Gas Production. *Catal. Rev.* **2007**, *49*, 511–560. [CrossRef]
4. Bradford, M.C.J.; Vannice, M.A. CO_2 Reforming of CH_4. *Catal. Rev. Sci. Eng.* **1999**, *41*, 1–42. [CrossRef]
5. Istadi, I.; Saidina Amin, N.A. Co-Generation of C_2 Hydrocarbons and Synthesis Gases from Methane and Carbon Dioxide: A Thermodynamic Analysis. *J. Natural Gas. Chem.* **2005**, *14*, 40–150.
6. Nikoo, M.K.; Amin, N.A.S. Thermodynamic analysis of carbon dioxide reforming of methane in view of solid carbon formation. *Fuel Proc. Technol.* **2011**, *92*, 678–691. [CrossRef]
7. Fraenkel, D.; Levitan, R.; Levy, M. A solar thermochemical pipe based on the CO_2-CH_4 (1:1) system. *Int. J. Hydrog. Energy* **1986**, *11*, 267–277. [CrossRef]
8. Pakhare, D.; Shaw, C.; Haynes, D.; Shekhawat, D.; Spivey, J. Effect of reaction temperature on activity of Pt- and Ru-substituted lanthanum zirconate pyrochlores ($La_2Zr_2O_7$) for dry (CO_2) reforming of methane (DRM). *J. CO_2 Util.* **2013**, *1*, 37–42. [CrossRef]
9. Wang, S.; Lu, G.Q.; Millar, G.J. Carbon Dioxide Reforming of Methane to Produce Synthesis Gas over Metal-Supported Catalysts: State of the Art. *Energy Fuels* **1996**, *10*, 896–904. [CrossRef]
10. Lang, J. Experimentelle Beiträge zur Kenntnis der Vorgänge bei der Wasser-und Heizgasbereitung. *Z. Phys. Chem.* **1888**, *2*, 161–183. [CrossRef]
11. Fischer, F.; Tropsch, H. Conversion of methane into hydrogen and carbon monoxide. *Brennst. Chem.* **1928**, *3*, 29.
12. Pakhare, D.; Spivey, J.J. A review of dry (CO_2) reforming of methane over noble metal catalysts. *Chem. Soc. Rev.* **2014**, *43*, 7813–7837. [CrossRef]
13. Aramouni, N.A.K.; Touma, J.G.; Abu Tarboush, B.; Zeaiter, J.; Ahmad, M. Catalyst design for dry reforming of methane: Analysis review. *Renew. Sustain. Energy Rev.* **2018**, *82*, 2570–2585. [CrossRef]
14. Papadopoulou, C.; Matralis, H.; Verykios, X. *Utilization of Biogas as a Renewewable Carbon Source: Dry Reforming of Methane, Catalysis for Alternative Energy Generation*; Guczi, L., Erdőhelyi, A., Eds.; Springer: Cham, Switzerland, 2012; pp. 57–127.
15. Singh, R.; Dhir, A.; Mohapatra, S.K.; Mahla, S.K. Dry reforming of methane using various catalysts in the process: Review. *Biomass Convers. Biorefinery* **2019**, *10*, 567–587. [CrossRef]
16. Papp, H.; Schuler, P.; Zhuang, Q. CO_2 reforming and partial oxidation of methane. *Top. Catal.* **1996**, *3*, 299–311. [CrossRef]
17. Mark, M.F.; Maier, W.F. CO_2-Reforming of Methane on Supported Rh and Ir Catalysts. *J. Catal.* **1996**, *164*, 122–130. [CrossRef]
18. Solymosi, F.; Kutsán, G.; Erdöhelyi, A. Catalytic reaction of CH_4 with CO_2 over alumina-supported Pt metals. *Catal. Lett.* **1991**, *11*, 149–156. [CrossRef]
19. Rostrup-Nielsen, J.R.; Hansen, J.H.B. CO_2-Reforming of Methane over Transition Metals. *J. Catal.* **1993**, *144*, 38–49. [CrossRef]
20. Ferreira-Aparicio, P.; Ruiz, A.G.; Rodriguez Ramos, I. Comparative study at low and medium reaction temperatures of syngas production by methane reforming with carbon dioxide over silica and alumina supported catalysts. *Appl. Catal. A Gen.* **1998**, *170*, 177–187. [CrossRef]
21. Ashcroft, A.T.; Cheetham, A.K.; Green, M.L.H.; Vernon, P.D.F. Partial oxidation of methane to synthesis gas using carbon dioxide. *Nature* **1991**, *352*, 225–226. [CrossRef]
22. Vernon, P.; Green, M.; Cheetham, A.; Ashcroft, A. Partial oxidation of methane to synthesis gas, and carbon dioxide as an oxidising agent for methane conversion. *Catal. Today* **1992**, *13*, 417–426. [CrossRef]
23. Takayasu, O.; Sato, F.; Ota, K.; Hitomi, T.; Miyazaki, T.; Osawa, T.; Matsuura, I. Separate production of hydrogen and carbon monoxide by carbon dioxide reforming reaction of methane. *Energy Convers. Manag.* **1997**, *38*, S391–S396. [CrossRef]
24. Qin, D.; Lapszewicz, J. Study of mixed steam and CO_2 reforming of CH_4 to syngas on MgO-supported metals. *Catal. Today* **1994**, *21*, 55l–560. [CrossRef]
25. Basini, L.; Sanfilippo, D. Molecular Aspects in Syn-Gas Production: The CO_2-Reforming Reaction Case. *J. Catal.* **1995**, *157*, 162–178. [CrossRef]
26. Bradford, M.C.; Vannice, M.A. The role of metal–support interactions in CO_2 reforming of CH_4. *Catal. Today* **1999**, *50*, 87–96. [CrossRef]
27. Barama, S.; Dupeyrat-Batiot, C.; Capron, M.; Bordes-Richard, E.; Bakhti-Mohammedi, O. Catalytic properties of Rh, Ni, Pd and Ce supported on Al-pillared montmorillonites in dry reforming of methane. *Catal. Today* **2009**, *141*, 385–392. [CrossRef]
28. Khani, Y.; Shariatinia, Z.; Bahadoran, F. High catalytic activity and stability of $ZnLaAlO_4$ supported Ni, Pt and Ru nanocatalysts applied in the dry, steam and combined dry-steam reforming of methane. *Chem. Eng. J.* **2016**, *299*, 353–366. [CrossRef]
29. Sakai, Y.; Saito, H.; Sodesawa, T.; Nozaki, F. Catalytic reactions of hydrocarbon with carbon dioxide over metallic catalysts. *React. Kinet. Catal. Lett.* **1984**, *24*, 253–257. [CrossRef]
30. Rezaei, M.; Alavi, S.M.; Sahebdelfar, S.; Yan, Z.-F. Syngas Production by Methane Reforming with Carbon Dioxide on Noble Metal Catalysts. *J. Nat. Gas. Chem.* **2006**, *15*, 327–334. [CrossRef]
31. Masai, M.; Kado, H.; Miyake, A.; Nishiyama, S.; Tsuruya, S. Methane Reforming by Carbon Dioxide and Steam Over Supported Pd, Pt, and Rh Catalysts. *Stud. Surf. Sci. Catal.* **1988**, *36*, 67–71. [CrossRef]
32. Tsyganok, A.I.; Inaba, M.; Tsunoda, T.; Hamakawa, S.; Suzuki, K.; Hayakawa, T. Dry reforming of methane over supported noble metals: A novel approach to preparing catalysts. *Catal. Commun.* **2003**, *4*, 493–498. [CrossRef]
33. Nematollahi, B.; Rezaei, M.; Khajenoori, M. Combined dry reforming and partial oxidation of methane to synthesis gas on noble metal catalysts. *Int. J. Hydrog. Energy* **2011**, *36*, 2969–2978. [CrossRef]

34. Vannice, M.A. The catalytic synthesis of hydrocarbons from H_2 CO mixtures over the group VIII metals: I. The specific activities and product distributions of supported metals. *J. Catal.* **1975**, *37*, 449–461. [CrossRef]
35. Solymosi, F.; Erdöhelyi, A. Hydrogenation of CO_2 to CH_4 over alumina-supported noble metals. *J. Mol. Catal.* **1980**, *8*, 471–474. [CrossRef]
36. Van Keulen, A.N.J.; Hegarty, M.E.; Ross, J.R.; Oosterkamp, P.F.V.D. The development of platinum-zirconia catalysts for the CO_2 reforming of methane. *Stud. Surf. Sci. Catal.* **1997**, *107*, 537–546. [CrossRef]
37. Anil, C.; Modak, J.M.; Madras, G. Syngas production via CO_2 reforming of methane over noble metal (Ru, Pt, and Pd) doped $LaAlO_3$ perovskite catalyst. *Mol. Catal.* **2020**, *484*, 110805. [CrossRef]
38. Ghelamallah, M.; Granger, P. Impact of barium and lanthanum incorporation to supported Pt and Rh on α-Al_2O_3 in the dry reforming of methane. *Fuel* **2012**, *97*, 269–276. [CrossRef]
39. Tsyganok, A.I.; Inaba, M.; Tsunoda, T.; Suzuki, K.; Takehira, K.; Hayakawa, T. Combined partial oxidation and dry reforming of methane to synthesis gas over noble metals supported on Mg–Al mixed oxide. *Appl. Catal. A Gen.* **2004**, *275*, 149–155. [CrossRef]
40. Perera, J.; Couves, J.W.; Sankar, G.; Thomas, J.M. The catalytic activity of Ru and Ir supported on Eu_2O_3 for the reaction, CO_2 + $CH_4 \rightleftharpoons 2\ H_2 + 2\ CO$: A viable solar-thermal energy system. *Catal. Lett.* **1991**, *11*, 219–225. [CrossRef]
41. De Caprariis, B.; de Filippis, P.; Palma, V.; Petrullo, A.; Ricca, A.; Ruocco, C.; Scarsella, M. Rh, Ru and Pt ternary perovskites type oxides BaZr(1-x)MeO_3 for methane dry reforming. *Appl. Catal. A Gen.* **2016**, *517*, 47–55. [CrossRef]
42. Yokota, S.; Okumura, K.; Niwa, M. Support Effect of Metal Oxide on Rh Catalysts in the CH_4-CO_2 Reforming Reaction. *Catal. Lett.* **2002**, *84*, 131–134. [CrossRef]
43. Zhang, Z.; Tsipouriari, V.; Efstathiou, A.M.; Verykios, X.E. Reforming of Methane with Carbon Dioxide to Synthesis Gas over Supported Rhodium Catalysts. *J. Catal.* **1996**, *158*, 51–63. [CrossRef]
44. Tsipouriari, V.; Efstathiou, A.; Zhang, Z.; Verykios, X. Reforming of methane with carbon dioxide to synthesis gas over supported Rh catalysts. *Catal. Today* **1994**, *21*, 579–587. [CrossRef]
45. Wang, H.Y.; Ruckenstein, E. Carbon dioxide reforming of methane to synthesis gas over supported rhodium catalysts: The effect of support. *Appl. Catal. A Gen.* **2000**, *204*, 143–152. [CrossRef]
46. Erdohelyi, A.; Cserenyi, J.; Solymosi, F. Activation of CH_4 and Its Reaction with CO_2 over Supported Rh Catalysts. *J. Catal.* **1993**, *141*, 287–299. [CrossRef]
47. Portugal, U.L.; Santos, A.C.S.F.; Damyanova, S.; Marques, C.M.P.; Bueno, J.M.C. CO_2 reforming of CH_4 over Rh-containing catalysts. *J. Mol. Catal. A Chem.* **2002**, *184*, 311–322. [CrossRef]
48. Sigl, M.; Bradford, M.C.J.; Knözinger, H.; Vannice, M.A. CO_2 reforming of methane over vanadia-promoted Rh/SiO_2 catalysts. *Top. Catal.* **1999**, *8*, 211–222. [CrossRef]
49. Bitter, J.H.; Seshan, K.; Lercher, J.A. Mono and Bifunctional Pathways of CO_2/CH_4 Reforming over Pt and Rh Based Catalysts. *J. Catal.* **1998**, *176*, 93–101. [CrossRef]
50. Nakamura, J.; Aikawa, K.; Sato, K.; Uchijima, T. Role of support in reforming of CH_4 with CO_2 over Rh catalysts. *Catal. Lett.* **1994**, *25*, 265–270. [CrossRef]
51. Nakamura, J.; Aikawa, K.; Sato, K.; Uchijima, T. The Role of Support in Methane Reforming with CO_2 over Rhodium Catalysts. *Stud. Surf. Sci. Catal.* **1993**, *90*, 495–500.
52. Drif, A.; Bion, N.; Brahmia, R.; Ojala, S.; Pirault-Roy, L.; Turpeinen, E.; Seelam, P.K.; Keiski, R.; Epron, F. Study of the dry reforming of methane and ethanol using Rh catalysts supported on doped alumina. *Appl. Catal. A Gen.* **2015**, *504*, 576–584. [CrossRef]
53. Bhat, R.; Sachtler, W. Potential of zeolite supported rhodium catalysts for the CO_2 reforming of CH_4. *Appl. Catal. A Gen.* **1997**, *150*, 279–296. [CrossRef]
54. Srimat, S.T.; Song, C. Effects of Pressure on CO_2 Reforming of CH_4 over Rh/Na-Y and Rh/Al_2O_3 Catalysts. *ACS Symp. Ser.* **2002**, *809*, 289–302.
55. Verykios, X.E. Mechanistic aspects of the reaction of CO_2 reforming of methane over Rh/Al_2O_3 catalyst. *Appl. Catal. A Gen.* **2003**, *255*, 101–111. [CrossRef]
56. Richardson, J.T.; Paripatyadar, S.A. Carbon dioxide reforming of methane with supported rhodium. *Appl. Catal.* **1990**, *61*, 293–309. [CrossRef]
57. Erdőhelyi, A.; Solymosi, F. Effect of the support on the adsorption and dissociation of CO and on the reactivity of surface carbon on Rh catalysts. *J. Catal.* **1983**, *84*, 446–460. [CrossRef]
58. Wei, J.; Iglesia, E. Structural requirements and reaction pathways in methane activation and chemical conversion catalyzed by rhodium. *J. Catal.* **2004**, *225*, 116–127. [CrossRef]
59. Sarusi, I.; Fodor, K.; Baán, K.; Oszkó, A.; Pótári, G.; Erdőhelyi, A. CO_2 reforming of CH_4 on doped Rh/Al_2O_3 catalysts. *Catal. Today* **2011**, *171*, 132–139. [CrossRef]
60. Wang, R.; Xu, H.; Liu, X.; Ge, Q.; Li, W. Role of redox couples of Rh^0/$Rh^{\delta+}$ and Ce^{4+}/Ce^{3+} in CH_4/CO_2 reforming over Rh–CeO_2/Al_2O_3 catalyst. *Appl. Catal. A Gen.* **2006**, *305*, 204–210. [CrossRef]
61. Djinovic, P.; Batista, J.; Pintar, A. Efficient catalytic abatement of greenhouse gases: Methane reforming with CO_2 using a novel and thermally stable Rh-CeO_2 catalyst. *Int. J. Hydrog. Energy* **2012**, *37*, 2699–2707. [CrossRef]
62. Djinovic, P.; Črnivec, I.G.O.; Batista, J.; Levec, J.; Pintar, A. Catalytic syngas production from greenhouse gasses: Performance comparison of Ru-Al_2O_3 and Rh-CeO_2 catalysts. *Chem. Eng. Process.* **2011**, *50*, 1054–1062. [CrossRef]

63. Solymosi, F.; Szőke, A.; Egri, L. Decomposition of methane and its reaction with CO_2 over Rh/ZSM-5 catalyst. *Top. Catal.* **1999**, *8*, 249–257. [CrossRef]
64. Pritchard, M.L.; McCauley, R.L.; Gallaher, B.N.; Thomson, W.J. The effects of sulfur and oxygen on the catalytic activity of molybdenum carbide during dry methane reforming. *Appl. Catal. A Gen.* **2004**, *275*, 213–220. [CrossRef]
65. Erdőhelyi, A.; Fodor, K.; Szailer, T. Effect of H_2S on the reaction of methane with carbon dioxide over supported Rh catalysts. *Appl. Catal. B Environ.* **2004**, *53*, 153–160. [CrossRef]
66. Szailer, T.; Novák, É.; Oszkó, A.; Erdőhelyi, A. Effect of H_2S on the hydrogenation of carbon dioxide over supported Rh catalysts. *Top. Catal.* **2007**, *46*, 79–86. [CrossRef]
67. Mancino, G.; Cimino, S.; Lisi, L. Sulphur poisoning of alumina supported Rh catalyst during dryreforming of methane. *Catal. Today* **2016**, *277*, 126–132. [CrossRef]
68. Matsui, N.; Anzai, K.; Akamatsu, N.; Nakagawa, K.; Ikenaga, N.; Suzuki, T. Reaction mechanisms of carbon dioxide reforming of methane with Ru-loaded lanthanum oxide catalyst. *Appl. Catal. A Gen.* **1999**, *179*, 247–256. [CrossRef]
69. Bradford, M.J.C.; Vannice, M.A. CO_2 Reforming of CH_4 over Supported Ru Catalysts. *J. Catal.* **1999**, *183*, 69–75. [CrossRef]
70. Nagaoka, K.; Okamura, M.; Aika, K. Titania supported ruthenium as a coking-resistant catalyst for high pressure dry reforming of methane. *Catal. Commun.* **2001**, *2*, 255–260. [CrossRef]
71. Ferreira-Aparicio, P.; Márquez-Alvarez, C.; Rodríguez-Ramos, I.; Schuurman, Y.; Guerrero-Ruiz, A.; Mirodatos, C. A Transient Kinetic Study of the Carbon Dioxide reforming of Methane over Supported Ru Catalysts. *J. Catal.* **1999**, *184*, 202–212. [CrossRef]
72. Ferreira-Aparicio, P.; Rodríguez-Ramos, I.; Anderson, J.A.; Guerrero-Ruiz, A. Mechanistic aspects of the dry reforming of methane over ruthenium catalysts. *Appl. Catal. A Gen.* **2000**, *202*, 183–196. [CrossRef]
73. Das, D.; Shah, M.; Gupta, R.K.; Bordoloi, A. Enhanced dry methane reforming over Ru decorated mesoporous silica and its kinetic study. *J. CO_2 Util.* **2019**, *29*, 240–253. [CrossRef]
74. Portugal, U.L., Jr.; Marques, C.M.P.; Araujo, E.C.C.; Morales, E.V.; Giotto, M.V.; Bueno, J.M.C. CO_2 reforming of methane over zeolite-Y supported ruthenium catalysts. *Appl. Catal. A Gen.* **2000**, *193*, 173–183. [CrossRef]
75. Safariamin, M.; Tidahy, L.H.; Abi-Aad, E.; Siffert, S.; Aboukaïs, A. Dry reforming of methane in the presence of ruthenium-based catalysts. *Comptes Rendus Chim.* **2009**, *12*, 748–753. [CrossRef]
76. Li, D.; Li, R.; Lu, M.; Lin, X.; Zhan, Y.; Jiang, L. Carbon dioxide reforming of methane over Ru catalysts supported on Mg-Al oxides: A highly dispersed and stable Ru/Mg(Al)O catalyst. *Appl. Catal. B Environ.* **2017**, *200*, 566–577. [CrossRef]
77. Kehres, J.; Jakobsen, J.G.; Andreasen, J.W.; Wagner, J.B.; Liu, H.; Molenbroek, A.; Sehested, J.; Chorkendorff, I.; Vegge, T. Dynamical Properties of a Ru/$MgAl_2O_4$ Catalyst during Reduction and Dry Methane Reforming. *J. Phys. Chem. C* **2012**, *116*, 21407–21415. [CrossRef]
78. Zhang, J.-C.; Ge, B.-H.; Liu, T.-F.; Yang, Y.-Z.; Li, B.; Li, W.-Z. Robust Ruthenium-Saving Catalyst for High-Temperature Carbon Dioxide Reforming of Methane. *ACS Catal.* **2020**, *10*, 783–791. [CrossRef]
79. Carrara, C.; Múnera, J.; Lombardo, E.A.; Cornaglia, L.M. Kinetic and Stability Studies of Ru/La_2O_3 Used in the Dry Reforming of Methane. *Top. Catal.* **2008**, *51*, 98–106. [CrossRef]
80. Carvalho, D.C.; de Souza, H.S.A.; Filho, J.M.; Oliveira, A.C.; Campos, A.; Milet, É.R.C.; de Sousa, F.F.; Padron-Hernandez, E.; Oliveira, A.C. A study on the modification of mesoporous mixed oxides supports for dry reforming of methane by Pt or Ru. *Appl. Catal. A Gen.* **2014**, *473*, 132–145. [CrossRef]
81. Gangwar, B.P.; Pentyala, P.; Tiwari, K.; Biswas, K.; Sharma, S.; Parag, A.; Deshpande, P.A. Dry reforming activity due to ionic Ru in $La_{1.99}Ru_{0.01}O_3$: The role of specific carbonates. *Phys. Chem. Chem. Phys.* **2019**, *30*, 16726–16736. [CrossRef]
82. Whang, H.S.; Choi, M.S.; Lim, J.; Kim, C.; Heo, I.; Chang, T.-S.; Lee, H. Enhanced activity and durability of Ru catalyst dispersed on zirconia for dry reforming of methane. *Catal. Today* **2017**, *293–294*, 122–128. [CrossRef]
83. Yu, Z.; Choi, K.; Rosynek, M.P.; Lunsford, J.H. From CH_4 reforming with CO_2 to pyrolysis over a platinum catalyst. *React. Kinet. Catal. Lett.* **1993**, *51*, 143–149. [CrossRef]
84. Bitter, J.H.; Hally, W.; Seshan, K.; van Ommen, J.G.; Lercher, J.A. The role of the oxidic support on the deactivation of Pt catalysts during the CO_2 reforming of methane. *Catal. Today* **1996**, *29*, 349–353. [CrossRef]
85. Bitter, J.H.; Seshan, K.; Lercher, J.A. Deactivation and Coke Accumulation during CO_2/CH_4 Reforming over Pt Catalysts. *J. Catal.* **1999**, *183*, 336–343. [CrossRef]
86. Bradford, M.J.C.; Vannice, M.A. CO_2 Reforming of CH_4 over Supported Pt Catalysts. *J. Catal.* **1998**, *173*, 157–171. [CrossRef]
87. Bitter, J.H.; Seshan, K.; Lercher, J.A. The State of Zirconia Supported Platinum Catalysts for CO_2/CH_4 Reforming. *J. Catal.* **1997**, *171*, 279–286. [CrossRef]
88. Bitter, J.H.; Seshan, K.; Lercher, J.A. On the contribution of X-ray absorption spectroscopy to explore structure and activity relations of Pt/ZrO_2 catalysts for CO_2/CH_4 reforming. *Top. Catal.* **2000**, *10*, 295–305. [CrossRef]
89. Nagaoka, K.; Seshan, K.; Aika, K.; Lercher, J.A. Carbon Deposition during Carbon Dioxide Reforming of Methane—Comparison between Pt/Al_2O_3 and Pt/ZrO_2. *J. Catal.* **2001**, *197*, 34–42. [CrossRef]
90. Souza, M.M.V.M.; Aranda, D.A.G.; Schmal, M. Reforming of Methane with Carbon Dioxide over Pt/ZrO_2/Al_2O_3 Catalysts. *J. Catal.* **2001**, *204*, 498–511. [CrossRef]
91. Reddy, G.K.; Loridanta, S.; Takahashi, A.; Delichčre, P.; Reddy, B.M. Reforming of methane with carbon dioxide over Pt/ZrO_2/SiO_2 catalysts-Effect of zirconia to silica ratio. *Appl. Catal. A Gen.* **2010**, *389*, 92–100. [CrossRef]

92. Özkara-Aydınoglu, S.; Özensoy, E.; Aksoylu, E. The effect of impregnation strategy on methane dry reforming activity of Ce promoted Pt/ZrO_2. *Int. J. Hydrog. Energy* **2009**, *34*, 9711–9722. [CrossRef]
93. Ballarini, A.D.; De Miguel, S.R.; Jablonski, E.L.; Scelza, O.A.; Castro, A.A. Reforming of CH_4 with CO_2 on Pt-supported catalysts Effect of the support on the catalytic behavior. *Catal. Today* **2005**, *107–108*, 481–486. [CrossRef]
94. Van Keulen, A.N.J.; Seshan, K.; Hoebink, J.H.B.J.; Ross, J.R.H. TAP Investigations of the CO_2 Reforming of CH_4 over Pt/ZrO_2. *J. Catal.* **1997**, *166*, 306–314. [CrossRef]
95. Nagaoka, K.; Seshan, K.; Lercher, J.A.; Aika, K. Activation mechanism of methane-derived coke (CH_x) by CO_2 during dry reforming of methane—Comparison for Pt/Al_2O_3 and Pt/ZrO_2. *Catal. Lett.* **2000**, *70*, 109–116. [CrossRef]
96. O'Connor, A.M.; Schuurman, Y.; Ross, J.R.H.; Mirodatos, C. Transient studies of carbon dioxide reforming of methane over Pt/ZrO_2 and Pt/Al_2O_3. *Catal. Today* **2006**, *115*, 191–198. [CrossRef]
97. Souza, M.M.V.M.; Martin Schmal, M. Combination of carbon dioxide reforming and partial oxidation of methane over supported platinum catalysts. *Appl. Catal. A Gen.* **2003**, *255*, 83–92. [CrossRef]
98. Damyanova, S.; Bueno, J.M.C. Effect of CeO_2 loading on the surface and catalytic behaviors of CeO_2-Al_2O_3-supported Pt catalysts. *Appl. Catal. A Gen.* **2003**, *253*, 135–150. [CrossRef]
99. Stagg, S.M.; Romeo, E.; Padro, C.; Resasco, D.E. Effect of Promotion with Sn on Supported Pt Catalysts for CO_2 Reforming of CH_4. *J. Catal.* **1998**, *78*, 137–145. [CrossRef]
100. García-Diéguez, M.; Pieta, I.S.; Herrera, M.C.; Larrubia, M.A.; Malpartida, I.; Alemany, L.J. Transient study of the dry reforming of methane over Pt supported on different γ-Al_2O_3. *Catal. Today* **2010**, *149*, 380–387. [CrossRef]
101. Da Fonseca, R.O.; Rabelo-Neto, R.C.; Simões, R.C.C.; Mattos, L.V.; Noronha, F.B. Pt supported on doped CeO_2/Al_2O_3 as catalyst for dry reforming of methane. *Int. J. Hydrog. Energy* **2020**, *45*, 5182–5191. [CrossRef]
102. Singh, S.A.; Madras, G. Sonochemical synthesis of Pt, Ru doped TiO_2 for methane reforming. *Appl. Catal. A Gen.* **2016**, *518*, 102–114. [CrossRef]
103. Nakagawa, K.; Anzai, K.; Matsui, N.; Ikenaga, N.; Suzuki, T.; Teng, Y.; Kobayashi, T.; Haruta, M. Effect of support on the conversion of methane to synthesis gas over supported iridium catalysts. *Catal. Lett.* **1998**, *51*, 163–167. [CrossRef]
104. Erdőhelyi, A.; Fodor, K.; Solymosi, F. Reaction of CH_4 with CO_2 and H_2O over supported Ir catalyst. *Stud. Surf. Sci. Catal.* **1997**, *107*, 525–530.
105. Maina, S.C.P.; Ballarini, A.D.; Vilella, J.I.; Sergio, R.; de Miguel, S.R. Study of the performance and stability in the dry reforming of methane of doped alumina supported iridium catalysts. *Catal. Today* **2020**, *344*, 129–142. [CrossRef]
106. Wei, J.; Iglesia, E. Structural and Mechanistic Requirements for Methane Activation and Chemical Conversion on Supported Iridium Clusters. *Angew. Chem. Int. Ed.* **2004**, *43*, 3685–3688. [CrossRef] [PubMed]
107. Wisniewski, M.; Boréave, A.; Gélin, P. Catalytic CO_2 reforming of methane over Ir/$Ce_{0.9}Gd_{0.1}O_{2-x}$. *Catal. Commun.* **2005**, *6*, 596–600. [CrossRef]
108. Wang, F.; Xu, L.; Zhang, J.; Zhao, Y.; Li, H.; Li, H.X.; Wu, K.; Xu, G.Q.; Chen, W. Tuning the metal-support interaction in catalysts for highly efficient methane dry reforming reaction. *Appl. Catal. B Environ.* **2016**, *180*, 511–520. [CrossRef]
109. Erdőhelyi, A.; Cserényi, J.; Papp, E.; Solymosi, F. Catalytic reaction of methane with carbon dioxide over supported palladium. *Appl. Catal. A Gen.* **1994**, *108*, 205–219. [CrossRef]
110. Shi, C.; Zhang, P. Effect of a second metal (Y, K, Ca, Mn or Cu) addition on the carbon dioxide reforming of methane over nanostructured palladium catalysts. *Appl. Catal. B Environ.* **2012**, *115–116*, 190–200. [CrossRef]
111. Singha, R.K.; Yadav, A.; Shukla, A.; Kumar, M.; Bal, R. Low temperature dry reforming of methane over Pd-CeO_2 nanocatalyst. *Catal. Commun.* **2017**, *92*, 19–22. [CrossRef]
112. Al-Doghach, F.A.J.; Rashid, U.; Zaina, Z.; Saiman, M.I.; Yap, Y.H.T. Influence of the Ce_2O_3 and CeO_2 promoters on the Pd/MgO catalyst in dry reforming of methane. *RSC Adv.* **2015**, *5*, 81739–81752. [CrossRef]
113. Panagiotopoulou, P.; Kondarides, D.I.; Verykios, X.E. Mechanistic Study of the Selective Methanation of CO over Ru/TiO_2 Catalyst: Identification of Active Surface Species and Reaction Pathways. *J. Phys. Chem. C* **2011**, *115*, 1220–1230. [CrossRef]
114. Lambeets, S.V.; Barroo, C.; Owczarek, S.; Jacobs, L.; Genty, E.; Gilis, N.; Kruse, N.; De Bocarmé, T.V. Adsorption and Hydrogenation of CO_2 on Rh Nanosized Crystals: Demonstration of the Role of Interfacet Oxygen Spillover and Comparative Studies with O_2, N_2O, and CO. *J. Phys. Chem. C* **2017**, *121*, 16238–16249. [CrossRef]
115. Van Tol, M.F.H.; Gielbert, A.; Nieuwenhuys, B.E. The adsorption and dissociation of CO_2 on Rh. *Appl. Surf. Sci.* **1993**, *67*, 166–178. [CrossRef]
116. Solymosi, F. The bonding, structure and reactions of CO_2 adsorbed on clean and promoted metal surfaces. *J. Mol. Catal.* **1991**, *65*, 337–358. [CrossRef]
117. Freund, H.-J.; Roberts, M.W. Surface chemistry of carbon dioxide. *Surf. Sci. Rep.* **1996**, *25*, 225–273. [CrossRef]
118. Campbell, C.T.; White, J.M. The adsorption, desorption, and reactions of CO and O_2 on Rh. *J. Catal.* **1978**, *54*, 289–302. [CrossRef]
119. Dubois, L.; Somorjai, G.A. The dissociative chemisorption of carbon dioxide on rhodium surfaces. *Surf. Sci.* **1979**, *88*, L13–L17. [CrossRef]
120. Dubois, L.H.; Somorjai, G.A. The chemisorption of CO and CO_2 on Rh (111) studied by high resolution electron energy loss spectroscopy. *Surf. Sci.* **1980**, *91*, 514–532. [CrossRef]
121. Weinberg, W.H. Why CO_2 does not dissociate on Rh at low temperature. *Surf. Sci.* **1983**, *128*, L224–L230. [CrossRef]

122. Goodman, D.W.; Peebles, D.E.; White, J.M. CO_2 dissociation on rhodium: Measurement of the specific rates on Rh(111). *Surf. Sci.* **1984**, *140*, L239–L243. [CrossRef]
123. Bradford, M.C.J.; Vannice, M.A. Metal-support interactions during the CO_2 reforming of CH_4 over model TiO_x/Pt catalysts. *Catal. Lett.* **1997**, *48*, 31–38. [CrossRef]
124. Kiss, J.; Révész, K.; Solymosi, F. Photoelectron spectroscopic studies of the adsorption of CO_2 on potassium-promoted Rh(111) surface. *Surf. Sci.* **1988**, *207*, 36–59. [CrossRef]
125. Liu, Z.M.; Zhou, Y.; Solymosi, F.; White, J.M. Vibrational study of CO_2 on potassium-promoted platinum (111). *J. Phys. Chem.* **1989**, *93*, 4383–4385. [CrossRef]
126. Hoffmann, F.M.; Weisel, M.D.; Paul, J. The activation of CO_2 by potassium-promoted Ru (001) I. FT-IRAS and TDMS study of oxalate and carbonate intermediates. *Surf. Sci.* **1994**, *316*, 277–293. [CrossRef]
127. Berkó, A.; Solymosi, F. Effects of potassium on the chemisorption of CO_2 and CO on the Pd (100) surface. *Surf. Sci.* **1986**, *171*, L498–L502. [CrossRef]
128. Solymosi, F.; Erdőhelyi, A.; Bánsági, T. Infrared study of the surface interaction between H_2 and CO_2 over rhodium on various supports. *J. Chem. Soc. Faraday Trans. 1 Phys. Chem. Condens. Phases* **1981**, *77*, 2645–2657. [CrossRef]
129. Heyl, D.; Rodemerck, U.; Bentrup, U. Mechanistic study of low-temperature CO_2 hydrogenation over modified Rh/Al_2O_3 catalysts. *ACS Catal.* **2016**, *6*, 6275–6284. [CrossRef]
130. Novák, É.; Fodor, K.; Szailer, T.; Oszkó, A.; Erdőhelyi, A. CO_2 hydrogenation on Rh/TiO_2 previously reduced at different temperatures. *Top. Catal.* **2002**, *20*, 107–117. [CrossRef]
131. De Leitenburg, C.; Trovarelli, A.; Kašpar, J. A Temperature-Programmed and Transient Kinetic Study of CO_2 Activation and Methanation over CeO_2 Supported Noble Metals. *J. Catal.* **1997**, *166*, 98–107. [CrossRef]
132. Beuls, A.; Swalus, C.; Jacquemin, M.; Hexen, G.; Karelovič, A.; Ruiz, P. Methanation of CO_2: Further insight into the mechanism over Rh/γ-Al_2O_3 catalyst. *Appl. Catal. B Environ.* **2012**, *113–114*, 2–10. [CrossRef]
133. Múnera, J.F.; Irusta, S.; Cornaglia, L.M.; Lombardo, E.A.; Ceesar, D.; Schmal, M. Kinetics and reaction pathway of the CO_2 reforming of methane on Rh supported on lanthanum-based solid. *J. Catal.* **2007**, *245*, 25–34. [CrossRef]
134. Pakhare, D.; Schwartz, V.; Abdelsayed, V.; Haynes, D.; Shekhawat, D.; Postonc, J.; Spivey, J. Kinetic and mechanistic study of dry (CO_2) reforming of methane over Rh-substituted $La_2Zr_2O_7$ pyrochlores. *J. Catal.* **2014**, *316*, 78–92.
135. Frennet, A. Chemisorption and Exchange with Deuterium of Methane on Metals. *Catal. Rev. Sci. Eng.* **1974**, *10*, 37–68.
136. Liao, M.-S.; Zhang, Q.-E. Dissociation of methane on different transition metals. *J. Mol. Catal. A Chem.* **1998**, *136*, 85–194. [CrossRef]
137. Klier, K.; Hess, J.S.; Herman, R.G. Structure sensitivity of methane dissociation on palladium single crystal surfaces. *J. Chem. Phys.* **1997**, *107*, 4033–4043. [CrossRef]
138. Belgued, M.; Pareja, P.; Amariglio, A.; Amariglio, H. Conversion of methane into higher hydrocarbons on platinum. *Nature* **1991**, *352*, 789–790. [CrossRef]
139. Solymosi, F.; Erdőhelyi, A.; Cserényi, J. A comparative study on the activation and reactions of CH_4 on supported metals. *Catal. Lett.* **1992**, *16*, 399–405.
140. Solymosi, F.; Erdőhelyi, A.; Cserényi, J.; Felvégi, A. Decomposition of CH_4 over supported Pd catalysts. *J. Catal.* **1994**, *147*, 272–278. [CrossRef]
141. Fernandez, C.; Miranda, N.; Garcia, X.; Eloy, P.; Ruiz, P.; Gordon, A.; Jimenez, R. Insights into dynamic surface processes occurring in Rh supported on Zr-grafted γ-Al_2O_3 during dry reforming of methane. *Appl. Catal. B Environ.* **2014**, *156–157*, 202–212.
142. Yamaguchi, A.; Iglesia, E. Catalytic activation and reforming of methane on supported palladium clusters. *J. Catal.* **2010**, *274*, 52–63. [CrossRef]
143. Hou, Z.; Chen, P.; Fang, H.; Zheng, X.; Yashima, T. Production of synthesis gas via methane reforming with CO_2 on noble metals and small amount of noble-(Rh-) promoted Ni catalysts. *Int. J. Hydrog. Energy* **2006**, *31*, 555–561. [CrossRef]
144. Wei, J.; Iglesia, E. Isotopic and kinetic assessment of the mechanism of methane reforming and decomposition reactions on supported iridium catalysts. *Phys. Chem. Chem. Phys.* **2004**, *6*, 3754–3759. [CrossRef]
145. Wei, J.; Iglesia, E. Reaction Pathways and Site Requirements for the Activation and Chemical Conversion of Methane on Ru-Based Catalysts. *J. Phys. Chem. B* **2004**, *108*, 7253–7262. [CrossRef]
146. Wei, J.; Iglesia, E. Mechanism and Site Requirements for Activation and Chemical Conversion of Methane on Supported Pt Clusters and Turnover Rate Comparisons among Noble Metals. *J. Phys. Chem. B* **2004**, *108*, 4094–4103. [CrossRef]
147. Mark, M.F.; Maier, W.F. Active Surface Carbon—A Reactive Intermediate in the Production of Synthesis Gas from Methane and Carbon Dioxide. *Angew. Chem. Int. Ed. Engl.* **1994**, *33*, 1657–1660. [CrossRef]
148. Matsui, N.; Nakagawa, K.; Ikenaga, N.; Suzuki, T. Reactivity of Carbon Species Formed on Supported Noble Metal Catalysts in Methane Conversion Reactions. *J. Catal.* **2000**, *194*, 115–121. [CrossRef]
149. Wang, H.Y.; Au, C.T. Carbon dioxide reforming of methane to syngas over SiO_2-supported rhodium catalysts. *Appl. Catal. A Gen.* **1997**, *155*, 239–252. [CrossRef]
150. Solymosi, F.; Erdőhelyi, A.; Kocsis, M. Surface Interaction between H_2 and CO_2 on Rh/AI_2O_3, Studied by Adsorption and Infrared Spectroscopic Measurements. *J. Catal.* **1980**, *65*, 428–436. [CrossRef]
151. Solymosi, F.; Erdőhelyi, A.; Lancz, M. Surface Interaction between H_2 and CO_2 over Palladium on Various Supports. *J. Catal.* **1985**, *95*, 567–577. [CrossRef]

152. Efstathiou, A.M.; Kladi, A.; Tsipouriari, V.A.; Verykios, X.E. Reforming of Methane with Carbon Dioxide to Synthesis Gas over Supported Rhodium Catalysts II. A Steady-State Tracing Analysis: Mechanistic Aspects of the Carbon and Oxygen Reaction Pathways to Form CO. *J. Catal.* **1996**, *158*, 64–75. [CrossRef]
153. Cornaglia, L.M.; Múnera, J.; Irusta, S.; Lombardo, E.A. Raman studies of Rh and Pt on La_2O_3 catalysts used in a membrane reactor for hydrogen production. *Appl. Catal. A Gen.* **2004**, *263*, 91–101. [CrossRef]
154. Aramouni, N.A.K.; Zeaiter, J.; Kwapinski, W.; Ahmad, M.N. Thermodynamic analysis of methane dry reforming: Effect of the catalyst particle size on carbon formation. *Energy Conv. Manag.* **2017**, *150*, 614–622. [CrossRef]
155. Tsipouriari, V.A.; Efstathiou, A.M.; Verykios, X.E. Transient Kinetic Study of the Oxidation and Hydrogenation of Carbon Species Formed during CH_4/He, CO_2/He, and CH_4/CO_2 Reactions over Rh/Al_2O_3 Catalyst. *J. Catal.* **1996**, *161*, 31–42. [CrossRef]
156. Schulz, L.A.; Kahle, L.C.S.; Delgado, K.H.; Schunk, S.A.; Jentys, A.; Deutschmann, O.; Lercher, J.A. On the coke deposition in dry reforming of methane at elevated pressures. *Appl. Catal. A Gen.* **2015**, *504*, 599–607. [CrossRef]
157. Rostrup-Nielsen, J.R. Aspects of CO_2-reforming of Methane. *Stud. Surf. Sci. Catal.* **1994**, *81*, 24–41.
158. Ferreira-Aparicio, P.; Fernandez-Garcia, M.; Guerrero-Ruiz, A.; Rodríguez-Ramos, I. Evaluation of the Role of the Metal–Support Interfacial Centers in the Dry Reforming of Methane on Alumina-Supported Rhodium Catalysts. *J. Catal.* **2000**, *190*, 296–308. [CrossRef]
159. Ghelamallah, M.; Granger, P. Supported-induced effect on the catalytic properties of Rh and Pt-Rh particles deposited on La_2O_3 and mixed α-Al_2O_3-La_2O_3 in the dry reforming of methane. *Appl. Catal. A Gen.* **2014**, *485*, 172–180. [CrossRef]
160. Raskó, J.; Solymosi, F. Reaction of adsorbed CH_3 species with CO_2 on Rh/SiO_2 catalyst. *Catal. Lett.* **1997**, *46*, 153–157. [CrossRef]
161. Schuurman, Y.; Marquez-Alvarez, C.; Kroll, V.C.H.; Mirodatos, C. Unraveling mechanistic features for the methane reforming by carbon dioxide over different metals and supports by TAP experiments. *Catal. Today* **1998**, *46*, 185–192. [CrossRef]